catalysts

MDPI

Review

A Critical Review of Photo-Based Advanced Oxidation Processes to Pharmaceutical Degradation

Isabelle M. D. Gonzaga, Caio V. S. Almeida and Lucia H. Mascaro *

Laboratory of Electrochemistry and Ceramics, Federal University of São Carlos, São Carlos 13565-905, SP, Brazil
* Correspondence: lmascaro@ufscar.br

Abstract: Currently, the production and consumption of pharmaceuticals is growing exponentially, making them emerging contaminants that cause hazards to the ecological environment and human health. These drugs have been detected in surface water and drinking water around the world. This indicates that the conventional treatments used are ineffective for the removal of these compounds from the water, since they are very complex, with high stability and have high persistence in aquatic environments. Considering this problem, several types of alternative treatments, such as advanced oxidative processes, have been studied. Of these, AOPs using irradiation have received increasing interest due to their fast reaction rate and the ability to generate oxidizing species, which leads to an efficient degradation and mineralization of organic compounds, thus improving the quality of water and allowing its reuse. Therefore, in this review, we focus on the advances made in the last five years of irradiated AOPs in the degradation of different classes of pharmaceutical compounds. The articles address different study parameters, such as the method of the synthesis of materials, oxidants used, treatment time, type of light used and toxicity of effluents. This review highlights the success of irradiated AOPs in the removal of pharmaceuticals and hopes to help the readers to better understand these processes and their limitations for removing drugs from the environment. It also sheds light on some paths that future research must follow so that the technology can be fully applied.

Keywords: degradation; photoelectrochemical; toxicity; enviroment

Citation: Gonzaga, I.M.D.; Almeida, C.V.S.; Mascaro, L.H. A Critical Review of Photo-Based Advanced Oxidation Processes to Pharmaceutical Degradation. *Catalysts* **2023**, *13*, 221. https://doi.org/10.3390/catal13020221

Academic Editors: Gassan Hodaifa, Rafael Borja and Mha Albqmi

Received: 20 December 2022
Revised: 12 January 2023
Accepted: 16 January 2023
Published: 18 January 2023

1. Introduction

Water pollution occurs when dangerous substances enter the oceans, rivers and lakes, among others, and can be found suspended or dissolved in these water bodies [1]. It is reported that areas of higher population density have a greater amount of water bodies polluted with different types of contaminants [2]. So, with the increase in human life expectancy, millions of medicines have been developed to maintain good health and quality of life [3]. In the last decades, pharmaceutical residues have been discovered in almost all different aquatic matrices on all continents [4]. Due to the high solubility and low biodegradability of the drugs, these compounds are extremely difficult to eliminate from water using conventional methods of treatment [5].

Existing wastewater treatment plants around the world are equipped with conventional treatment methods for the removal of simple organic substances, such as filtration, sedimentation, flocculation, adsorption and/or biological treatment [6]. However, these methods do not completely destroy organic pharmaceutical pollutants. Therefore, many researchers are in a relentless search for unconventional methods for pharmaceutical remediation in wastewater. Advanced oxidation processes (AOPs) are becoming attractive alternative techniques due to the promising chance of complete removal of drugs with production of non-toxic by-products [7].

AOPs are based on the generation of strong oxidants capable of oxidizing a wide range of organic compounds with one or several double bonds [8], such as process thermal, electrochemical, sonochemical, transition metal-based and irradiated. Of these, irradiated AOPs have been highlighted (Figure 1). Irradiated AOPs are green processes that do not involve secondary pollution, have mild reaction conditions, are easy to operate and have high pollutant degradation efficiency [9,10].

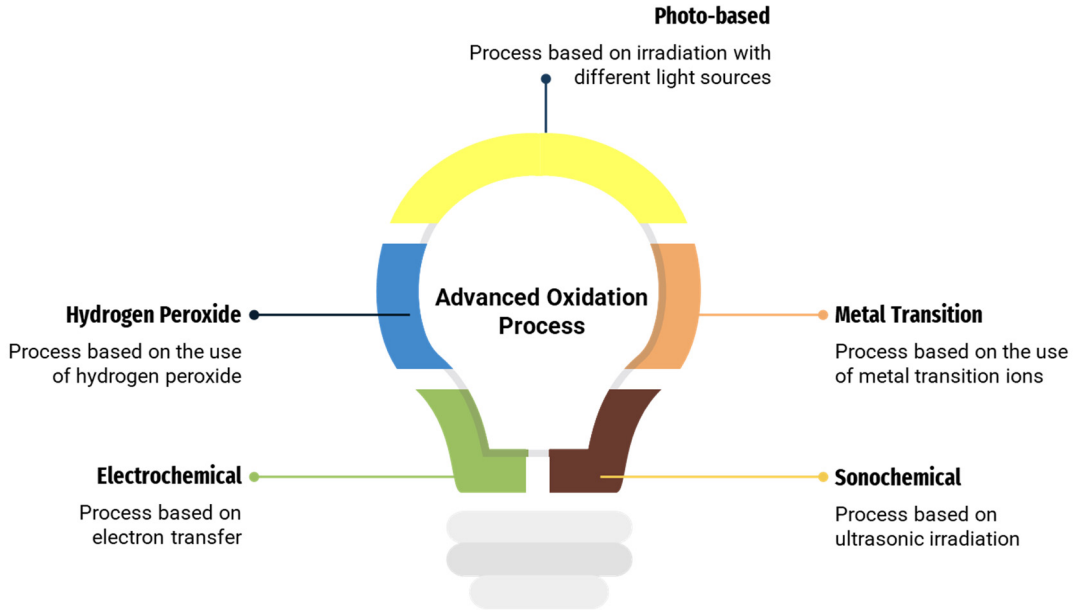

Figure 1. Different advanced oxidative process for the removal of pharmaceuticals.

This review aims to provide a discussion of recent literature that uses irradiated AOPs to potentiate radicals formation to completely remove drugs and/or transform by-products into less toxic by-products. Research works that produce new materials, study different techniques for removing drugs and/or evaluate the toxicity of effluents after treatment are discussed. Additionally, the treatment of water contaminated with various drugs is examined, which is classified according to the functional group. Thus, six different classes are approached, namely the nitrogenated, chlorinated, fluorinated, sulfured, phosphorated and oxygenated. Finally, a critical discussion of these approaches is also presented for a better understanding of the gaps opened in this topic in the literature.

2. Status of Pharmaceutical Pollution

Water is one of the most important compounds on the planet, as it is directly related to the existence of living beings. With the growth of the world population and the development of technology, water pollution has become a very important issue. Water contamination can be the result of several factors; one of the most polluting is the rapid development of industries and, consequently, the disposal of industrial waste [11]. Among the existing hazardous effluents, we can see that pharmaceutical products often play a vital role in the emission of toxic substances into the environment [12]. Drugs, which are organic and/or inorganic chemical compounds, can be classified according to their therapeutic actions as antibiotics, analgesics, beta-blockers, anesthetics, radiographic contrast agents and antidepressants [13].

Drugs have received enormous attention regarding detection and degradation due to their potential adverse effects on humans and the ecosystem [14]. Thus, the non-treatment of waste with antibiotics can give rise to antibiotic-resistant bacteria. Another class of drugs can cause various other problems, such as the development of reproductive disorders, birth defects, severe bleeding, cancer, organ damage, endocrine disorders and

toxic effects on aquatic organisms, which could have immeasurable consequences for humanity [15]. In Table 1, it is possible to observe widely used drugs, which have been covered in the literature.

Table 1. Drugs reported in the literature as objects of study for removal in wastewater.

Class	Pharmaceuticals	Abbreviation	Chemical Formula	Use
NITROGENATED	Acetaminophen	ACT	$C_8H_9NO_2$	Analgesic and antipyretic for mild pain and fever
	Tramadol	TRA	$C_{16}H_{25}NO_2$	Analgesic for rigorous pain
	Azithromycin	AZT	$C_{38}H_{72}N_2O_{12}$	Antibiotic used to treat respiratory, ear, skin or sexually transmitted infections
	Doxorubicin	DOX	$C_{27}H_{29}NO_4$	Antibiotic used for the therapy of lymphoma, leukemia and sarcoma
	Metronidazole	MTZ	$C_6H_9N_3O_3$	Antiparasitics and antiprotozoa
	Trimethoprim	TRIM	$C_{14}H_{18}N_4O_3$	Antibiotic used for mild-to-moderate bacterial infections
	Caffeine	CAF	$C_8H_{10}N_4O_2$	Used for mild pain and is mostly consumed in the form of coffee
	Propranolol	PROP	$C_{16}H_{21}NO_2$	Used for hypertension, cardiac arrhythmias, angina and hyperthyroidism
CHLORINATED	Lamotrigine	LAM	$C_9H_7Cl_2N$	Used to fight seizures
	Chloramphenicol	CAP	$C_{11}H_{12}Cl_2N_2O_5$	Antibiotics used for severe or life-threatening infections
	Diclofenac	DIC	$C_{14}H_{11}Cl_2NO_2$	Used for the therapy of mild-to-moderate acute pain
	Indomethacin	IDM	$C_{19}H_{16}ClNO$	Used for inflammatory arthritis
	Chlorhexidine	CLH	$C_{22}H_{30}Cl_2N_{10}$	Used topical antiseptic and dental practice for the treatment of dental inflammation
	Clorazepate	CLZ	$C_{16}H_{11}ClN_2O_3$	Anticonvulsant for therapy in epilepsy and as an anxiolytic
	Hydroxyzine	HDZ	$C_{21}H_{27}ClN_2O_2$	Used largely for symptoms of allergy, nausea and anxiety
	Indapamide	IDP	$C_{16}H_{16}ClNO_3$	Antihypertensive and a diuretic
	Bezafibrate	BZF	$C_{19}H_{20}ClNO_4$	Used for hyperlipidemia
FLUORATED	Ciprofloxacin	CIP	$C_{17}H_{18}FN_3O_3$	Used in the therapy of mild-to-moderate urinary or respiratory infections
	Ofloxacin	OFLO	$C_{18}H_{20}FN_3O_4$	Used for treatment rare instances of hepatocellular injury
	Enrofloxacin	ENR	$C_{19}H_{22}FN_3O_3$	Antibiotic used to treat infections of the urinary system
	Levofloxacin	LEV	$C_{18}H_{20}FN_3O_4$	Antibiotic used to treat infections, such as pneumonia and sinusitis
	Etofinamate	ETO	$C_{18}H_{18}F_3NO_4$	Used in the treatment of muscles and joints
	Fluoxetine	FLU	$C_{17}H_{18}F_3NO$	Used to treat major depressive, moderate-to-severe bulimia and obsessive-compulsive disorder
SULFURATED	Eprosartan	EPS	$C_{23}H_{24}N_2O_4S$	Used for the treatment of high blood pressure
	Captopril	CPT	$C_9H_{15}NO_3S$	Used in the therapy of hypertension
	Sulpiride	SUL	$C_{15}H_{23}N_3O_4S$	Used therapy as an antidepressant

	Sulfamonomethoxine	SFX	$C_{11}H_{12}N_4O_3S$	Long acting antibacterial agent
	Amoxicillin	AMX	$C_{16}H_{19}N_3O_5S$	Used in the treatment of mild-to-moderate bacterial infections
PHOSPORATED	Ifosfamide	IFD	$C_7H_{15}C_{l2}N_2O_2P$	Chemotherapy used to treat certain types of cancer, such as cancer of the ovary and cervix
	Cyclophosphamide	CFD	$C_7H_{15}C_{l2}N_2O_2P$	Cyclophosphamide is used to treat cancer of the ovaries, breast, blood and lymph systems
OXIGENATED	Aspirin	AAS	$C_9H_8O_4$	Used as a medicine to treat pain, fever and inflammation
	Ketoprofen	KET	$C_{16}H_{14}O_3$	Anti-inflammatory, with analgesic, anti-inflammatory and antirheumatic effects
	Naproxen	NAP	$C_{14}H_{14}O_3$	Analgesic for pain
	Ibuprofen	IBU	$C_{13}H_{18}O_2$	Anti-inflammatory used to treat pain and fever

These compounds are recalcitrant towards conventional treatment methods commonly used (sedimentation, flocculation, adsorption and ultrafiltration, for example), which are efficient for the removal of simple substances and materials on a macro/micro scale, while the advanced oxidation processes utilize the high reactivity of oxidants to degrade organic compounds to harmless products in water progressively have shown better efficiency in degrading these drugs. The combination of two or more AOPs is increasingly promising since, in some cases, only one AOPs is not enough to mineralize the effluent. Thus, combining technologies is a promising alternative for complete drug removal.

3. Photocatalysis as a Tool for the Degradation of Different Pharmaceuticals

3.1. Nitrogenous-Based Compounds

Pharmaceuticals that have heterocyclic compounds with nitrogen, such as pyridine, are widely used in living beings. Some examples of commonly used nitrogenous drugs are acetaminophen, metronidazole, tramadol and azithromycin, among others [16]. Heterocyclic nitrogenous compounds have high toxicity and recalcitrance and there are reports of frequent detection occurring in the aquatic environment, and thus the existing treatment methods are not efficient [17]. Thus, it is necessary to seek efficient systems for the complete mineralization of these compounds during water treatment processes.

In this sense, Li et al. [18] studied the photodegradation of acetaminophen (ACT) by combining UV light with different oxidants, such as chloramine, hydrogen peroxide and persulfate. The researchers showed that the drug can be effectively degraded by the combined processes when compared to the exclusive use of UV irradiation and oxidants. When comparing the efficiency of the three hybrid methods, they found that the efficiency was given in the following order: UV-LED/Persulfate > UV-LED/Hydrogen peroxide > UV-LED/Chloramines. Furthermore, it was observed that the kinetics of acetominophen removal increased when the oxidant dosage was increased in all cases. Finally, acute toxicity tests carried out using *Vibrio fisheri* and UV-LED/Persulfate were more efficient. In this view, persulfate was found as the most promising oxidant for the combination with UV-LED in the degradation of acetaminophen. On the other hand, Cai and co-workers carried out work investigating the efficiency of ACT removal with thermal treatment/peroxymonosulfate (T/PMS). They achieved efficient removal of the compound. Comparing the works that use T/PMS [19–21] with photo-assisted works [18,22], it was observed that the light-based processes more efficiently remove the toxicity of the studied effluents.

More recently, Qiangwei Li and co-workers [22] investigated the use of the Co_3O_4/TiO_2 heterojunction to degrade ACT through the photocatalytic activation of the sulfite. They discovered through X-ray photoelectron spectroscopy analysis and theoretical calculations that electron transfer from Co_3O_4 to TiO_2 directly contributes to the catalytic activation of the sulfite. Therefore, due to the unique configuration, 96% of ACMPH was removed in just 10 min. Showing that sulfite radicals activation is extremely promising.

Another widely used nitrogenated compound, azithromycin, is a common antibiotic, and during the COVID-19 pandemic, its use increased even more. Therefore, it is extremely important to search for new technologies to remove this antibiotic. Thus, Sayadi et al. [23] investigated the synthesis of a new material with iron, zinc and tin oxide to apply it to the photocatalytic removal of azithromycin. The effect of pH, contact time, catalyst content and the initial concentration of azithromycin was analyzed, and under optimal conditions (pH = 3, 120 min with 1 g/L of catalyst), obtained 90.06% of azithromycin degraded under UVC irradiation.

More recently, Tenzi and co-workers [24] studied a new material for photodegradation with UV-LED from AZT, $SrTiO_3$. In its optimal condition, with 40 mg of the material and 4 h of treatment, 99% of drug removal occurred. The authors justified its excellent performance through two important factors: (i) the nanostructured and irregular morphology and (ii) the hole action and hydroxyl formation.

Another drug in this important class is metronidazole. In this sense, Martins et al. [25] studied the synthesis of ginite with different alkaline hydroxides (Na, Li and K) and subsequently applied it to remove metronidazole using photo-Fenton technology. The authors reported that cations directly influence the morphology of the material, resulting in different surface areas. Na@giniita showed the largest surface area, 10.9 $m^2 g^{-1}$, when compared to the others. When applying them in the degradation, Na@giniita obtained 91% degradation, so the authors concluded that the greater the surface area, the more efficient the removal of MTZ.

Still, Neghi and collegues [26] carried out the removal of the MTZ, but unlike the previous works cited, they carried out the degradation on a laboratory scale (Figure 2a) and on a pilot scale (Figure 2b). They used different methodologies, such as Persulfate (PS), TiO_2 activated by UV-C (UV/TiO_2), PS activated by UV-C (UV/PS) and UV/PS with TiO_2 ($UV/PS/TiO_2$). The great difficulty was optimizing the parameters, since the scales of the systems were very different. In the optimized condition, which was the combination of the three technologies, regardless of the system used, 90% of the MTZ was removed. In addition, toxicity studies using Vibrio Fisheri were performed and, in addition to antibiotic removal, effluent toxicity was removed.

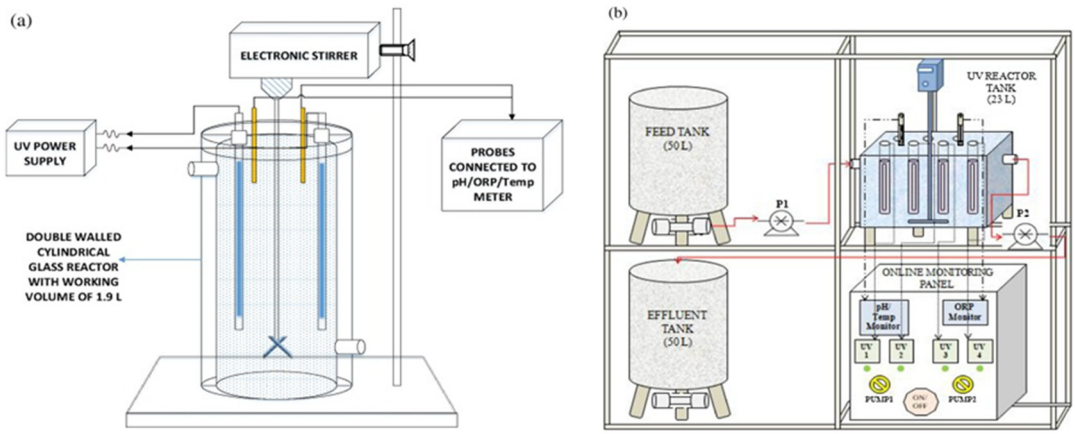

Figure 2. Comparison of photodegradation systems used with UV, PS or TiO_2, single or coupled. (**a**) laboratory scale and (**b**) pilot scale. Reprinted with permission from [26]. Copyright © 2023 Elsevier Ltd.

3.2. Chlorinated-Based Compounds

Chloramphenicol (CAP), Diclofenac (DC), Hydroxyzine (HDZ) and Indomethacin (IMT), among others, are drugs widely used worldwide. In this context, Leeladevi et al. [27] proposed the $SmVO_4$/g-C_3N_4 synthesis using a simple hydrothermal method. Due to the excellent photocatalytic activity, when the material was applied for CAP removal it achieved 94.35% efficiency. The excellent performance was justified by its unique composition and an excellent metal-free decorated photocatalyst alternative. Additionally, Hu and co-workers [28] studied a new strategy, photocatalysis coupled with microbial fuel cell (photo-MFC) on a Ni/Ti_2O_3 photocathode to increase the degradation efficiency of CAP. It was observed that the best degradation efficiency of CAP can reach 82.62% removal. Finally, the evaluation of the ecotoxicity of the degradation products showed that the degradation of CAP in the photo-MFC system modified with Ni/Ti_2O_3 presented a remarkable trend towards low toxicity levels. Therefore, it represents a very promising system for industrial waste degradation.

Kumar et al. [29] reported the synthesis of a Fe_3O_4@$SrTiO_3$/$Bi_4O_5I_2$ heterojunction through a hydrothermal process. The heterojunction was used for DC removal under simulated sunlight irradiation. Current results reveal that the optimized heterojunction exhibited a 98.4% removal of diclofenac within 90 min. EPR analyzes show that OH and O_2 radicals are present in DC degradation. The improved performance was justified by the proposal of a Z scheme (Figure 3), since the charge separation was obviously improved and facilitated by Fe_3O_4 and Ti^{4+}/Ti^{3+}, the involved redox couples. Thus, the authors demonstrate a promising material for rational design and fabrication of semiconductor heterojunctions for environmental applications.

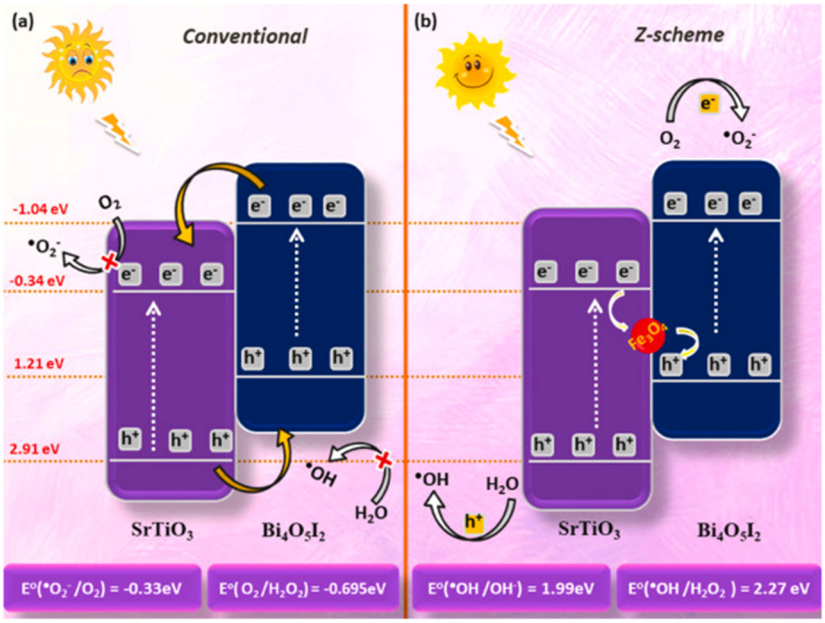

Figure 3. (**a**,**b**) Photocatalytic mechanism Z proposed by Kumar et al. Reprinted with permission from [29]. Copyright © 2023 Elsevier Ltd.

Examining Table 2, it is possible to conclude that the degradation of nitrogenous and chlorinated base compounds was successfully degraded via photo-assisted and photocatalytic AOPs systems. New materials and technologies were proposed to improve the removal rate and mineralization of the systems. Still, few works carry out their tests on a pilot scale.

Table 2. Selected recent studies of AOPs photo-irradiated processes for nitrogenated and chlorated base compound removal.

Pharmaceutical	Process	Experimental Conditions	Results	Ref.
DC	Photocatalysis	pH = 3; t = 150 min; [Catalyst] = 0.1 g L^{-1}; [DC] = 60 mg L^{-1}	99.4% DC and 87.8% TOC removal	[30]
CAP	Electrochemical and photo-assisted	pH = 6.8; t = 8h; [CAP] = 50 mg L^{-1}	100% CAP removal and complete removal of antibiotic activity	[31]
IMT	Photocatalysis	pH = 6.8; t = 45 min; [Catalyst] = 0.03 g mL^{-1}; [IMT] = 20 mg L^{-1}	97.3% IMT removal	[32]
IMT	UV–vis/peroxydisulfate	pH = 7; t = 45 min; [PDS] = 20 μM [IMT] = 20 μM	~80% IMT and 30% TOC removal	[33]
MET	Photocatalysis	pH = 2; t = 15 min; [Catalyst] = 1.2 g L^{-1} [MET] = 10 mg L^{-1}	94.3% MET removal	[34]
DC	US/photo-Fenton	pH = 3; t = 90 min; [Fe^{2+}] = 0.20 mg L^{-1}; [H_2O_2] = 1 mg L^{-1}; [DC] = 1 mg L^{-1}	94.4% DC and 17% TOC removal	[35]
AZT	Photocatalysis	t = 8h; [Catalyst] = 2 mg mL^{-1} [AZT] = 20 mg L^{-1}	90% AZT removal and complete removal of toxicity	[36]
AZT	UV/H_2O_2	pH = 9; t = 120 min; [H_2O_2] = 482 mg L^{-1}; [DC] = 1 mg L^{-1}	53% AZT and 100% TOC removal	[37]
CAF	Fenton, photo-Fenton, UV/H_2O_2 and UV/Fe^{3+}	pH = 5.8; t = 120 min; [H_2O_2] = 0.5 mL L^{-1}; [CAF] = 20 mg L^{-1}	99% CAF removal	[38]
LEV	Photo-electrocatalyst	pH = 5.9; t = 4 h; [LEV] = 20 mg L^{-1}	99% LEV and 100% TOC removal	[39]

3.3. Fluorinated-Based Compounds

Fluoroquinolones (FQ) are a family of fluorinated-based antibiotics used for both human and animal extensively. Most common FQs used include CIP, ENR, NOR and others [40–42]. They all present a bicyclic core structure related to the substance 4-quinolone with a fluorine substituted on the C6 position. FQs are incompletely metabolized in bodies and excreted into wastewaters. Because of the incomplete removal in conventional wastewater treatment facilities, since these treatment plants were never designed to deal with antibiotics, FQs are released to the environment via wastewater discharge on a continuous basis [42]. In recent years, these substances were detected in other aqueous environments around the world, such as lakes, rivers, seas, ground water and even in tap water [41–45].

Thus, it is crucial to develop efficient and economical treatment technologies to eliminate FQs from natural waters and wastewaters due to the potential threats of FQs to aquatic ecosystems and human beings. Photodegradation was found to be an important mechanism responsible for their removal in surface waters. The quinolone chromophore group enables the molecules to absorb UV-A light efficiently [46].

In this sense, Geng and co-workers [40] investigated the photo-degradation of three FQs (NOR, CIP, LEV) by VUV/UV and UV irradiation. They evaluated several effects such as flow rate (30, 60 and 90 L h^{-1}), FQs initial concentration (15, 30 and 60 μmol L^{-1}), temperature (5, 15, 25, 35 and 45 °C), initial pH (ranging 3 to 11) and typical anions in degradation. FQs was degraded more efficiently with high temperatures and low initial

concentration (Figure 4a). The effect of the flow rate was small and exhibited a maximum value at around 60 L h^{-1} (Figure 4a). In the pH range of 3–9, the photo-degradation rate constants of NOR and CIP increased with the pH but decreased at pH 11, which was related to different dissociation forms in the water at different pH. However, the photo-degradation kinetic constant of LEV was slightly affected by pH in the VUV/UV system (Figure 4c). In the VUV/UV system, carbonate and phosphate species enhanced the removal rate of FQs. However, sulfate, chloride and nitrate restrained the degradation process of FQs (Figure 4b,d).

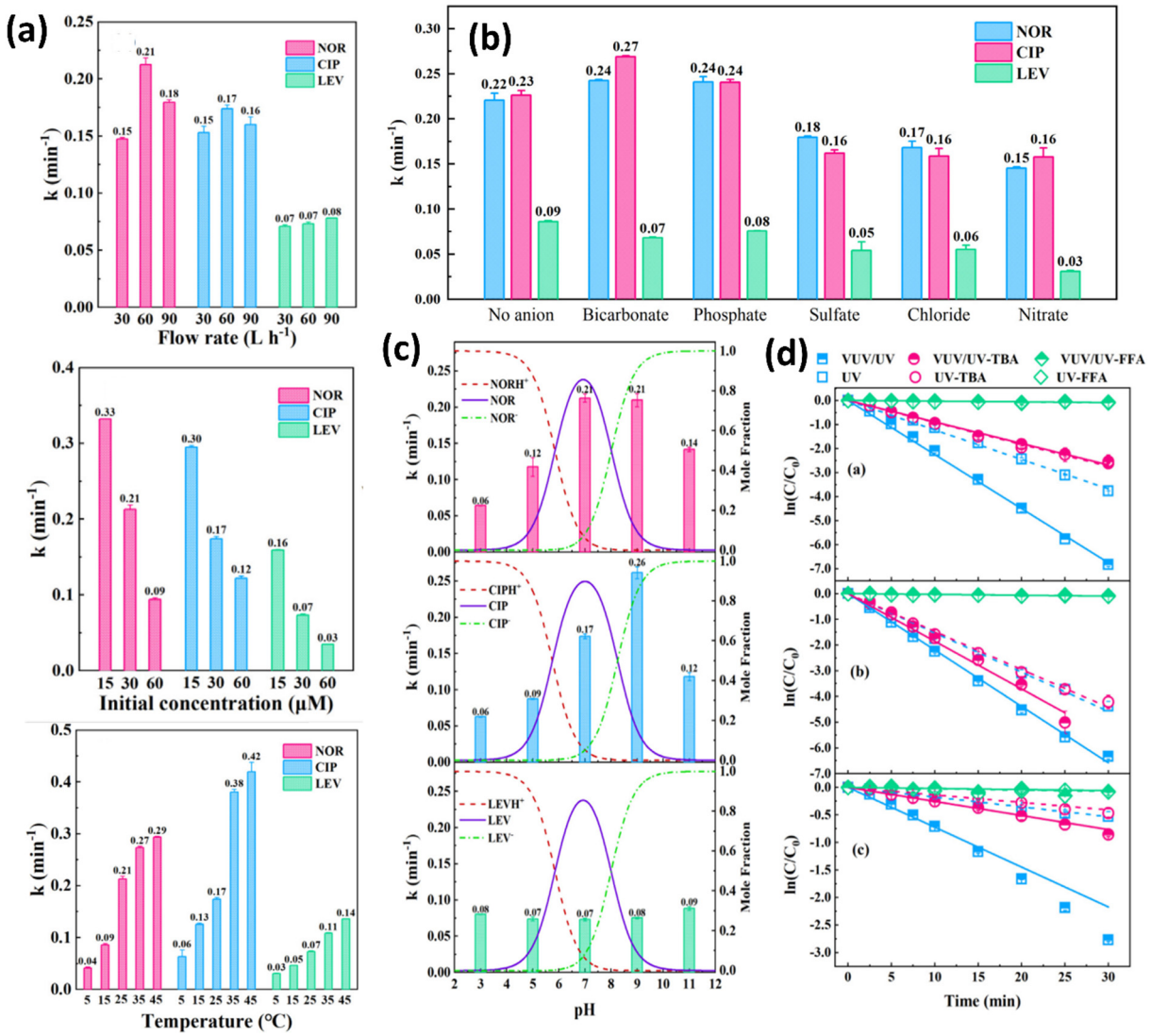

Figure 4. Comparison of the first-order rate constants of three FQs by the VUV/UV irradiation processes in pure water with various factors. (**a**) Flow rate; initial concentration of FQs and temperature; (**b**) effect of anion on the photodegradation of FQs; (**c**) initial pH and chemical specifications of the FQs; (**d**) degradation of the three antibiotics by UV and VUV/UV. Conditions: temperature = 25 °C, pH = 7.0 ± 0.05; [FQs] = 30 μmol L^{-1}; flow rate = 60 L h^{-1}; [Anion] = 300 μmol L^{-1}; [TBA] = 100 mmol L^{-1}. Reprinted with permission from [40]. Copyright © 2023 Elsevier Ltd.

The photo-degradation mechanisms of FQs in the VUV/UV system involved the direct photolysis, O_2 and OH oxidation. The degradation pathways of FQs were defluorination, decarboxylation and piperazine ring oxidation, and demethylation was a particular degradation pathway for LEV. In addition, antibacterial activities significantly decreased in the VUV/UV process due to defluorination and decarboxylation induced by VUV and OH. Particularly, the comparison of the energy cost showed that the VUV/UV process was

more energy efficient than UV process, indicating that the VUV/UV system was a promising treatment technology for removing FQs from water or wastewater [40].

In another work, Mondal, Saha, and Sinha [47] studied the degradation of ciprofloxacin by using various AOPs, such as UV, H_2O_2, UV/H_2O_2, modified Fenton (nanoscale zero-valent iron-nZVI/H_2O_2) and modified photo-Fenton at near neutral pH. The degradation of CIP by photolysis was performed at the initial pH of 7 and with the initial concentration of 10 mg L^{-1}. Approximately 60% of the antibiotic was removed within 120 min, confirming ciprofloxacin as a photosensitive compound. However, only 4% of the total organic carbon (TOC) removal was achieved, indicating that the degradation of CIP by UV irradiation may not prove to be feasible in 120 min. Later, hydrogen peroxide (H_2O_2) with several concentrations was added to ciprofloxacin solution (10 mg L^{-1}) in presence of UV light at initial pH 7. The TOC % removal increased from 10.47% for only H_2O_2 to 35.41% for UV/H_2O_2 combination due to a higher amount of hydroxyl radicals (OH) generation due to photolysis.

The UV/H_2O_2 combination was highly effective in achieving 100% removal efficiency of CIP in 40 min for higher doses of H_2O_2 (100 mmol L^{-1}), while the modified photo-Fenton oxidation process using 100 mmol L^{-1} of H_2O_2 and nZVI dose of 5 mmol L^{-1} was capable of completely removing ciprofloxacin in 30 min. Additionally, this combination reached the highest percentage of mineralization, removing 60% of the initial TOC. According to the authors, the degradation of ciprofloxacin may occur through: (i) the reaction at the piperazinyl ring; (ii) the oxidation of quinolone moiety, thereby leading to defluorination and hydroxyl substitution reaction; and (iii) the oxidation of the cyclopropyl group, resulting in ring cleavage.

In summary, the use of photolysis was not sufficient to completely remove CIP as it requires a high reaction time and has a very low mineralization rate. On the other hand, the UV/H_2O_2 method could be suited for complete removal of ciprofloxacin in comparison to the modified Fenton and modified photo-Fenton oxidation process as there is no sludge formation; however, it may require a high dose of H_2O_2 [47].

In an interesting work, Liu et al. [48] studied the degradation behavior of OFLO and Levofloxacin LEV using UV/H_2O_2 and UV/PS. The effects of oxidant dose (50 to 300 μmol·L^{-1}), solution pH (3 to 11) and coexisting substances (such as Cl^-, NO_3^-, SO_4^{2-}, Ca^{2+}, Mg^{2+} and NOMs (nature organic matters)) were investigated. The addition of H_2O_2 or PS significantly improves the degradation efficiency of OFLO and LEV (5 mg L^{-1}), while UV/PS achieves a better degradation effect than UV/H_2O_2 under the same oxidant concentration. The removal efficiencies of OFLO and LEV were 96.40% and 99.23% with PS concentration of 150 μmol·L^{-1}, where the removal efficiencies were 22.52 and 13.11 times as high as that of UV process, respectively (pH = 3 and t = 30 min). The degradation of both OFLO and LEV revealed pronounced pH dependence in UV/H_2O_2 and UV/PS processes, where the impact on LEV was greater than that on OFLO, indicating that LEV might be more easily degraded due to its shorter half-life. The TOC removal efficiencies of OFLO and LEV were 36.24% and 38.36%, respectively, for the UV/H_2O_2 system. By contrast, the UV/PS system exhibited the highest activity for the mineralization of OFL and LEV, with TOC removal efficiency of about 46.43% and 49.74%, respectively, indicating that $SO_4^{\cdot-}$ generated in the UV/PS process yields a greater mineralization of antibiotics than OH in the UV/H_2O_2 process.

The coexisting substances (Cl^-, NO_3^- and NOM) exhibited more inhibition regarding the degradation of OFLO and LEV in the UV/H_2O_2 than the UV/PS system. SO_4^{2-} has negligible influence on the UV/H_2O_2 processes, while it showed positive effect on UV/PS degradation. The results of acute toxicity assay demonstrated that OFLO exhibited higher acute toxicity than LEV, while the triphenyl tetrazolium chloride (TTC) dehydrogenase activity of the intermediate products of OFLO was lower than LEV [48].

Recently, Wang and co-workers [49] reported the fast removal, after 4 min, and high mineralization (63.3% at 8 min) of 45 μmol L^{-1} norfloxacin at neutral pH by the VUV/Fe^{2+}/H_2O_2 system (90 μmol L^{-1} Fe^{2+} and 3 mmol L^{-1} H_2O_2). Compared with other UV-

based and VUV-based systems (UV, UV/H_2O_2, UV/Fe^{2+}/H_2O_2, VUV, UV/Fe^{2+}, VUV/H_2O_2, VUV/Fe^{2+}/H_2O_2), the VUV/Fe^{2+}/H_2O_2 system increased the pseudo-first-order reaction rate constant of NOR removal by 2.3–14.9 times; increased the mineralization by 20.4–59.4%; and reduced the residual ratio of H_2O_2 by 19.9−70.1%. Moreover, HO·, O^{-2} and singlet oxygen ($^1O_2$) were the main ROS during NOR removal at neutral pH. The degradation pathways of NOR included defluorination, attack by HO·, decarboxylation and piperazine ring conversion by O_2^-. Moreover, adding Fe^{2+} to the VUV/H_2O_2 system reduced cost by 36.8%, 36.2% and 36.2% in ultrapure water, tap water and secondary wastewater, respectively. As a result, the VUV/Fe^{2+}/H_2O_2 process also achieved the rapid removal of NOR in real waters at neutral pH, while saving considerable cost and manifesting the feasibility of VUV/Fe^{2+}/H_2O_2 system in real waters.

Some researchers have studied the feasibility of O_3 and UV treatment (independent or together) to remove antibiotic wastewaters [50–53]. Liu et al. [50] investigated the degradation and mineralization of CIP in high-salinity wastewater through ozonation coupled with UV. Compared with independent O_3 (37.5%), the dissolved organic carbon (DOC) reduction was significantly increased by the introduction of UV irradiation (91.4%), which was attributed to the process of UV catalyzing O_3 to produce a reactive oxygen species (ROS), including OH, O_2 and $^1O_2$. The existence of salinity (3.5%, *w*/*v*) accelerated O_3 mass transfer at the gas–liquid interface, so CIP degradation was boosted by 17.7% and 2.0% in O_3/SO_4^{2-} and O_3/Cl^- system, respectively, within 15 min. The pH had little impact on the salt-free and O_3/containing Na_2SO_4 system. On the contrary, for an O_3/containing NaCl system, CIP and DOC removal was promoted with the increase of pH from 3 to 11 due to O_3 mass-transfer rate enhancement. The results of LC-MS demonstrated that the dominant reaction site of CIP in the UV/O_3 process was the piperazine ring. The toxicity of products decreased significantly as compared with the parent pollutant, which proved that the UV/O_3 process was promising in the hyper-salinity industry.

Paucar et al. [52] examined the effectiveness of the UV/O_3 process on the removal of personal care products (PPCPs) in the secondary effluent of a municipal wastewater treatment plant (WWTP). Experiments were conducted using a pilot-scale treatment process with two flow-through reactors, equipped with three 65 W lamps (UV_{65W}), connected in series. Ozone dosage (1–4 and 6 mg L^{-1}) and hydraulic retention time (HRT; 5 and 10 min). Of the 38 PPCPs detected, 11 were antibiotics, with ciprofloxacin and levofloxacin highlighted. In this system, ciprofloxacin was degraded below it limit of detection (LOD) at the ozone dose of 1 mg L^{-1} in 5 min. However, levofloxacin required an ozone dose of 6 mg L^{-1} to be degraded below LOD. The authors attributed the difference in the efficiency of treatment to the chemical properties of contaminants and highlighted further comprehensive studies in the areas of the reaction kinetics, the formation of byproducts, possible pathways and toxicity of wastewater treated by the UV/O_3 system.

Heterogeneous photocatalysis is a promising technique capable of directly attacking pollutant molecules and generating OH radicals and superoxides (O_2^-), powerful oxidants capable of destroying pollutants and transforming them into water and carbon dioxide [54]. Many studies developed photocatalysts with higher yields and easier operation [54–57].

Costa and co-workers [55] reported the ciprofloxacin photodegradation TiO_2/SnO_2 nanocomposites as heterogenous photocatalysts. The photocatalytic experiments were studied at different variables, such as catalyst dosage, drug concentration and pH solution. Titanate nanotubes (Na-TiNT) were synthesized using the hydrothermal method and then modified with Sn^{2+} using the coprecipitation method. Therefore, photolysis showed the small removal of CIP (4.63%) over 120 min of exposure time under UV-light radiation while the removal of CIP for Na-TiNT, SnO_2 and TiO_2/SnO_2 nanocomposites were 41.55%, 45.83% and 92.8%, respectively (Figure 5a). Increasing the catalyst dosage of TiO_2/SnO_2 nanocomposite from 25 to 50 mg (Figure 5b) in the CIP photodegradation increased the degradation rate of 27.8% to 92.8%, respectively. The authors attributed this behavior to high surface for interaction with CIP molecules and effective photon

absorption. In contrast, increasing the catalyst amount to 75 mg, decreased the degradation rate for CIP, which was related to the increase of the opacity of the solution. The best photocatalytic performance was achieved at pH 7, where 97.7% of CIP molecules were oxidized (Figure 5c). In addition, the initial concentration of CIP had little influence on the removal of the compound. The study of radical scavengers indicated that the oxygen singlets, holes and superoxide radicals are the main species associated with the CIP photodegradation (Figure 5d)

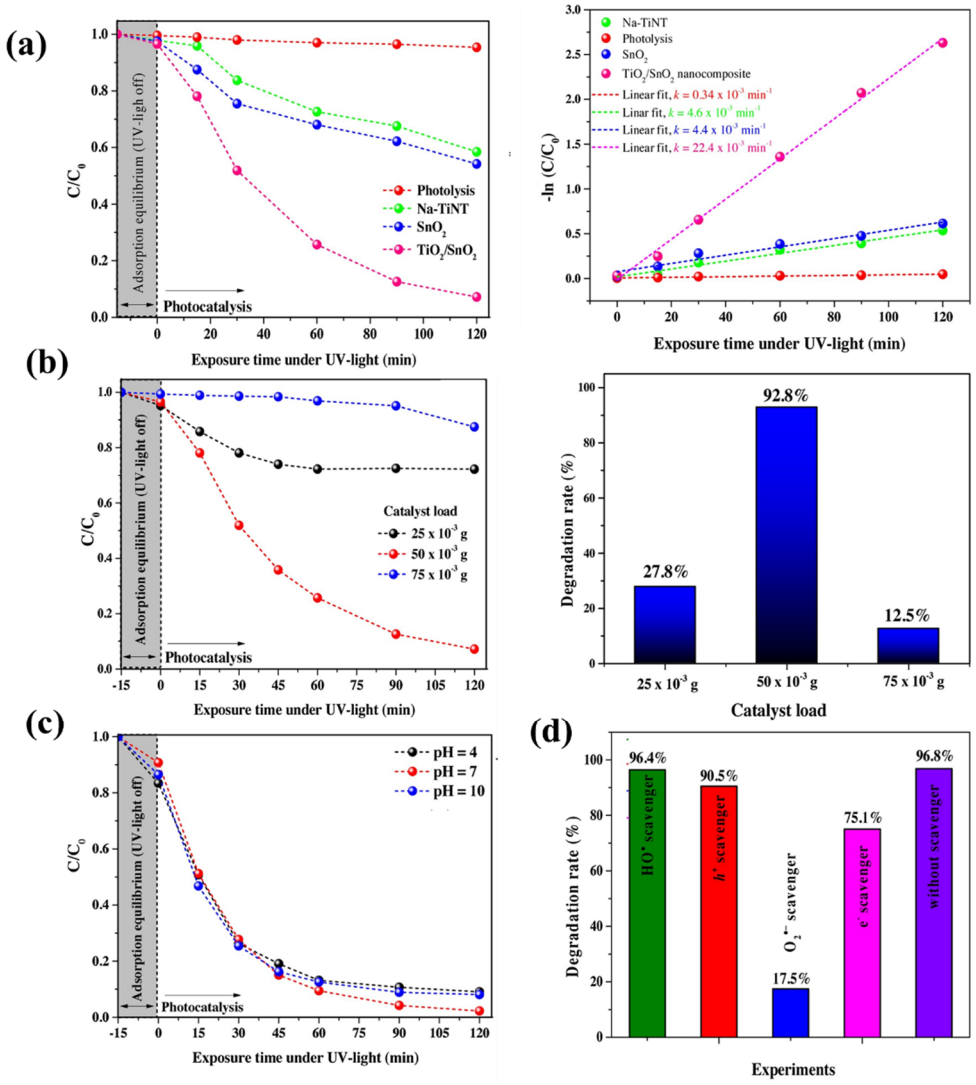

Figure 5. (**a**) Kinects study by the photocatalytic degradation curve and –ln(C/C0) curve against exposure time (t) for ciprofloxacin using Na-TiNTs, SnO_2 and TiO_2/SnO_2 samples as photocatalyst. (**b**) Degradation rate, for different amounts of TiO_2/SnO_2 nanocomposite (25×10^{-3} g, 50×10^{-3} g and 75×10^{-3} g) against 120 min of exposure time. (**c**) Photocatalytic performance for TiO_2/SnO_2 nanocomposite at different initial pH values of ciprofloxacin solution. (**d**) Degradation rate at the end of 120 min, using different radicals scavengers. Reprinted with permission from [55]. Copyright © 2023 Elsevier Ltd.

The results presented in the photodegradation of ciprofloxacin from TiO_2/SnO_2 nanocomposite [55] were promising in comparison with other works in the literature [56–59]. Nguyen et al. [59] reported the optimal CIP degradation rates of 78.7% using co-doped TiO_2 nanomaterials (N, S-TiO_2) at pH 5.5, a catalyst dosage of 50 mg and CIP initial concentration of 30 mg L^{-1}. Similar results were obtained by Zhang et al. [57] using Vo-WO_3/Bi_2WO_6 composites under visible light. They achieved 79.5% of CIP removal within 120 min under visible light irradiation (a 300 W Xe lamp) when 40 mg of the photocatalyst

was added into CIP solution (10 mg L^{-1}). According to the active species-capturing results and ESR test, h^+ and $\cdot O_2^-$ played crucial roles in photodegradation CIP, while OH played a weak role [57].

Moreover, Wu and co-workers [58], proposed an intercalated heterostructural g-C_3N_4/TiO_2 supported on Halloysite nanotubes (HNTs) and obtained 87% of CIP removal (15 mg L^{-1}), employing a 300W Xe lamp after 60 min of irradiation. In addition, the main active species of g-C_3N_4-TiO_2/HNTs heterojunction composites were $\cdot O_2^-$ and the h^+ in the process of photocatalytic degradation, in agreement with the results presented by Zhang et al. [57]. Despite the promising results, the authors did not evaluate the toxicity of the by-products formed nor the rates of mineralization achieved, fundamental parameters to determining the efficiency of degradation.

In another research, Prabavathi et al. [59] demonstrated a novel Sm_6WO_{12} decorated g-C_3N_4 heterojunction for the degradation of levofloxacin (10 mg L^{-1}) in the aqueous phase. TEM images confirmed the formation of heterostructure between the C_3N_4 nanosheets and Sm_6WO_{12} nanorods. The Sm_6WO_{12}/g-C_3N_4 nanocomposite heterojunction catalyst shows higher photocatalytic efficiency towards LEV degradation (90.8%, after 70 min), which was 20.52 and 2.93 times higher than individual Sm_6WO_{12} and g-C_3N_4, respectively. Based on the radical trapping experiments analysis, O_2^- and OH were the main reactive species for the degradation of LEV. Through CG-MS, the authors identified that the intermediate steps of levofloxacin included the decarboxylation reaction of the methyl- morpholine group followed by the degradation of the N-methyl piperazine ring, dealkylation defluorination and hydroxylation. The degradation might be continued with the breakdown of intermediates to small molecule organic acids as well as pollutant mineralization.

Several other compounds were used for the removal of levofloxacin under solar irradiation, reaching different percentages of degradation under different conditions [60–63]. For example, Zhang et al. [62] reported the removal of 89.2% of the LEV in water within 75 min under simulated sunlight using the Bi_2O_3/P-C_3N_4 composite. Further, through radicals capture, electron spin resonance (ESR) and the density functional theory (DFT) experiments verified the mechanism of the heterojunction degradation of LEV and revealed that holes and superoxide free radicals are the main active substances in the degradation of LEV. Finally, eleven intermediate products were identified and four possible degradation pathways were proposed. According to the authors, the entire degradation process mainly occurs in the quinolone and piperazinyl groups. The first pathway is the dehydrogenation of LEV followed by the piperazine oxidation and ring opening and then the oxidation for continuous CO removal. The third degradation pathway included the hydroxylation of LEV, oxidative decarboxylation and, furthermore, the demethylation of the methyl group on the piperazine ring. The fourth degradation path is the decarboxylation of LEV which is further oxidatively demethylated. The further degradation mechanism may be mainly manifested as the further opening of the quinolone group and oxazine ring (the degradation produces small molecules of amine compounds and carboxylic acid compounds). Finally, H_2O, CO_2 and other small molecules are generated.

Al Balushi et al. [60] achieved a 70% degradation rate of LEV (5 mg L^{-1}) after 240 min of treatment using visible light from LEDs (455 nm). The generation of hydroxy radicals was attributed as the main driver of pharmaceutical photodegradation. Upon illumination with visible light, electrons are excited from the valence band to the conduction band of the CdS microspheres. The holes created on the valence band migrate to the surface and scavenge water molecules to generate OH·radicals. The highly oxidizing radicals can degrade the pharmaceuticals. The electrons on the other hand may scavenge adsorbed molecular oxygen to form superoxide radicals ($O_2\cdot$) that oxides water to form OH· radicals that can perform the pharmaceutical photodegradation.

While Lu et al. [61] employing $CeVO_4$-$BiVO_4$ nanocomposites, removed 95.7% of LEV after 300 min using 50 mg L^{-1} of the pollutant. According to the authors, the higher photodegradation activity for LEV degradation for the $CeVO_4$-$BiVO_4$ heterojunction, in

comparison to bare photocatalyst material, is a result of the enhancement of separation and transfer efficiency of photogenerated electron–hole pairs. The trapping experiments and ESR tests identified that the contribution of active species was in the descending order of $OH > h^+ > O_2^-$. In all cases, the possible degradation of intermediate products and paths of LEV was similar to the one reported by Prabavathi et al. [59].

Fluoxetine (FLU) is another fluorinated-based antidepressant (trade name Prozac®) that gained considerable attention since it was detected in surface waters and has the potential to be bioaccumulated [63]. In regards to this, several researchers investigated the removal of FLU by UV and other photo-assisted AOPs with different degradation rates [64–68]. For example, Pan and co-workers [64] investigated the toxicity of FLU and the products formed during UV photolysis by using zebrafish embryos (*Danio rerio*) as a model. The degradation rates of FLU for five days were approximately 63.6 ± 2.14%, 84.6 ± 0.99% and 97.5 ± 0.25% after 15, 30 and 60 min of UV irradiation, respectively. Using LC-MS measurements and density flooding theory (DFT) theoretical calculations, two possible degradation pathways for FLU were proposed: In pathway I, the 4O–12C in the structure of FLU was broken in the presence of UV irradiation. In pathway II, the fluorine atom passing through the parent molecule of FLU was defluorinated under UV irradiation and hydroxylated via hydroxyl substitution process. According to the results of the toxicity evaluation of the possible degradation intermediates, the byproducts retained certain biological toxicity. The authors highlighted the need to consider the toxicity of mixtures and the formation and persistence of toxicologically relevant degradation products when assessing environmental risk.

Hollman, Dominic and Achari [65] presented an evaluation of the UV/PAA (peracetic acid) process for the degradation of four pharmaceuticals venlafaxine (VEN), sulfamethoxazole (SFX), fluoxetine (FLU) and carbamazepine (CBZ) with comparison to UV/H_2O_2 process. All pharmaceuticals tested in this study were degraded below detection limits by UV/PAA (λ = 254 nm), following pseudo-first-order kinetics. Increasing PAA and H_2O_2 dosage (between 5 and 100 mg L^{-1}) or UVC intensity (between 650 and 3500 W m^{-3}) resulted in a linear increase in pseudo-first-order rate coefficients. UV/H_2O_2 was found to be more efficient than UV/PAA for the degradation of FLU, VEN and CBZ. While UV/PAA was more effective in SFX degradation. Mass spectrum analysis revealed that the FLU mineralization pathway included hydroxylated FLU formed as a result of primary attack by·OH, which was also reported in previous studies on the degradation of FLU using UV/H_2O_2 and UV/TiO_2 [66]. The primary attack of the OH on FLU could possibly target any of the open sites on both the benzene rings to form numerous monohydrated isomers, and the possibility of substitution of trifluoromethyl group also exists [66].

The use of semiconductor photocatalysis is another strategy proposed to improve the fluoxetine degradation. In this context, Sharma et al. [67] reported the construction of the hybrid heterojunction of Fe_3O_4-$BiVO_4$/$Cr_2V_4O_{13}$ (FBC) for visible and solar photo-degradation of FLU. Within 60 min of visible exposure, 99.2% of FLU was removed at pH 7. The high total organic carbon removal of 80.3% and 61.4% by FBC under visible and solar light confirmed the mineralization after 180 min of treatment. Scavenging experiments and the electron spin resonance (ESR) probe suggest OH and O_2^- radicals as the dominant species.

More recently, Norouzi and co-workers [68] studied FLU removal via anodic oxidation, employing different anodes Ti/RuO_2, Ti/RuO_2-IrO_2 and Ti/RuO_2-IrO_2-SnO_2 and graphite and carbon nanotubes (CNTs) as cathodes. The effect of current intensity (from 100 to 50 mA), initial pH (2, 4, 6, 8 and 10), initial FLU concentration (from 50 to 25 mg L^{-1}) and process time (40, 80, 120, 160 and 200 min) on FLU removal efficiency was investigated. Previous, all electrode combinations used (anode + cathode) were tested under the same conditions (current intensity = 300 mA, $[FLU]_0$ = 20 mg L^{-1}, time = 160 min and pH 6) to determine the optimal electrode. The Ti/RuO_2–IrO_2–SnO_2 was chosen as the optimal anode, and the CNTs were selected as the optimal cathode in the AO process for FLU removal. The results showed that at current intensity, pH, initial FLU concentration and process time of 500 mA, 6, 25 mg L^{-1} and 160 min, respectively, maximum FLU removal

efficiency was observed, which was 96.25%. The TOC results demonstrated that about 81.51% of the mineralization of the FLU was achieved after 6 h under optimal experimental conditions. GC-MS results also showed that no toxic intermediates formed.

From Table 3, it is possible to state that the degradation of fluorinated-based compounds was successfully degraded via photo-combined AOPs systems. Different approaches were utilized, such as UV/H_2O_2, UV/O_3 and semiconductor materials. Despite the low rate of the removal and mineralization of the compounds using only UV radiation, the photocoupled systems showed high rates of removal and mineralization.

However, most of these systems still do not use real samples or large-scale flow reactors.

Table 3. Selected recent studies of photo-assisted AOPs processes for fluorinated and sulfurized base compounds removal.

Pharmaceutical Compound	Process	Experimental Conditions	Results	Ref.
NOR, CIP and LEV	VUV/UV and UV irradiation	pH = 7 Flow rate: 60 L h^{-1} [NOR] = [CIP] = [LEV] = 15 μmol L^{-1} T = 45 °C	The compounds were degraded more efficiently with high temperature and low initial concentration. The degradation pathways of FQs were defluorination, decarboxylation and piperazine ring oxidation, and demethylation was a particular degradation pathway for LEV.	[40]
CIP	UV, H_2O_2, UV/H_2O_2, modified Fenton and modified photo-Fenton	pH = 7 [CIP] = 10 mg L^{-1} [H_2O_2] = 100 mmol L^{-1} [nZVI] = 5 mmol L^{-1}	Only 4% of TOC removal for UV radiation TOC removal % increased from 10.47% for only H_2O_2 to 35.41 % for UV/H_2O_2. nZVI/H_2O_2 removed 100% of CIP in 30 min and 60% of the initial TOC.	[47]
OFLO and LEV	UV/H_2O_2 and UV/PS	pH = 3 [LEV] = [OFLO] = 5 mg L^{-1} t = 30 min [H_2O_2] = [PS] = 150 μmol·L^{-1}	The removal efficiencies of OFLO and LEV were 96.40% and 99.23% with UV/PS. The TOC removal efficiencies of OFLO and LEV were 36.24% and 38.36%, respectively, for the UV/H_2O_2 system. By contrast, the UV/PS system exhibited mineralization of OFL and LEV, with TOC removal efficiency about 46.43% and 49.74%, respectively.	[48]
NOR	UV, UV/H_2O_2, UV/Fe^{2+}/H_2O_2, VUV, UV/Fe^{2+}, VUV/H_2O_2, VUV/Fe^{2+}/H_2O_2	pH = 7 [NOR] = 45μmol L^{-1} [Fe^{2+}] = 90 μmol L^{-1} [H_2O_2] = 3 mmol L^{-1}	VUV/Fe^{2+}/H_2O_2 process removed 100% of NOR after 4 min, and high mineralization (63.3% at 8 min) and achieved rapid removal of NOR in real waters at neutral pH.	[49]
CIP	UV/O_3	pH = 5.6 Gas flow: 0.5 L min^{-1} [CIP] = 100.0 mg L^{-1} [O_3] = 30.0 ± 2.0 mg L^{-1} min^{-1}	Compared with single O_3 (37.5%), the DOC reduction was prompted significantly by the introduction of UV irradiation (91.4%) within 40 min. The toxicity of products decreased significantly as compared with parent pollutant.	[51]
38 PPCPs, highlighting CIP and LEV	UV/O_3	Ozone dosage (1−4 and 6 mg L^{-1}) and hydraulic retention time (5 and 10 min)	CIP was degraded below the limit of detection (LOD) at the ozone dose of 1 mg L^{-1} in 5 min. However, LEV required an O_3 dose of 6 mg L^{-1} to be degraded below LOD.	[52]

CIP	Photolysis	pH = 7 catalyst dosage = 50 mg [CIP] = 5 mg L^{-1}	Photolysis showed a small removal of CIP (4.63%) over 120 min of exposure time under UV-light radiation while the removal of CIP for Na-TiNT, SnO_2 and TiO_2/SnO_2 nanocomposite were 41.55%, 45.83% and 92.8%, respectively.	[55]
LEV	Photocatalysis	[LEV] = 10 mg L^{-1} catalyst dosage = 50 mg	The Sm_6WO_{12}/g-C_3N_4 nanocomposite heterojunction catalyst shows higher photocatalytic efficiency towards LEV degradation (90.8%, after 70 min).	[59]
FLU	UV photolysis	pH = 7 T = 20 °C [FLU] = 1 mg L^{-1} Irradiation source = 300 W	The degradation rates of FLU for five days were approximately 63.6% ± 2.14%, 84.6% ± 0.99%, and 97.5% ± 0.25% after 15, 30 and 60 min of UV irradiation, respectively.	[64]
VEN, SFX, FLU and CBZ	UV/PAA and UV/H_2O_2	pH = 7 UVC intensity = 3.50 kW m^{-3} [PAA] = [H_2O_2] = 50 mg L^{-1} [compound] = 10 mg L^{-1}	UV/H_2O_2 was found to be more efficient than UV/PAA for the degradation of FLU, VEN and CBZ. While UV/PAA was more effective in SFX degradation.	[65]
FLU	Photocatalysis	pH = 7 [FLU] = 10 mg L^{-1} Light source = 280 mW cm^{-1} catalyst dosage = 0.3 mg mL^{-1}	Within 60 min of visible exposure, 99.2% of FLU was removed at pH 7. The high total organic carbon removal of 80.3% and 61.4% by FBC under visible and solar light confirmed the mineralization after 180 min of treatment.	[67]
FLU	Ti/RuO_2, Ti/RuO_2-IrO_2 and Ti/RuO_2-IrO_2-SnO_2	pH = 6 i = 500 mA [FLU] = 25 mg L^{-1} t = 160 min	At optimized conditions, maximum FLU removal efficiency was observed, which was 96.25%. The TOC results showed that about 81.51% of the mineralization of the FLU was achieved after 6 h under optimal experimental conditions.	[68]
SMZ, SDZ and SML	UV, UV/H_2O_2 and UV/$K_2S_2O_8$	pH = 7 [SMZ]=[SDZ]=[SML] 15 mg L^{-1} [H_2O_2] = [$K_2S_2O_8$] = 4.4 × 10^{-4} M	UVC proved inadequate in removing these compounds. A concentration of 4.4 × 10^{-4} mol L^{-1} of H_2O_2 or $K_2S_2O_8$ increases SMZ degradation up to 100%. UVC/PDS requires less energy than UVC and UVC/H_2O_2 system.	[69]
SMX	UVC/VUV	pH = 7 [SMX] = 100 mg L^{-1}, Fluence = 54.9 mJ cm^{-2}	Total SMX removal was reached at a fluence of 54.9 mJ cm^{-2}, while the TOC removal of 98.5% was attained at fluence of 109.8 mJ cm^{-2}.	[70]
SMT	photo-Fenton	pH = 4 [SMT] = 1.8 × 10^{-2} mmol L^{-1} [H_2O_2] = 0.74 mmol L^{-1} [Fe^{3+}] = 0.25 mmol L^{-1}	The mineralization of SMT were significantly enhanced in the VUV/UV photo-Fenton process as compared to the UV and UV photo-Fenton processes after 60 min of treatment, achieving ~60% of TOC removal.	[71]
DF, SP, SMX and SIM	photo-Fenton	[H_2O_2] = 100 mmol L^{-1} [pharmaceuticals] = 20 mg L^{-1}, Fe^{2+} dosage = 1/200 mol L^{-1} of $FeSO_4$ $7H_2O$ and H_2O_2 UV intensity = 75 mW cm^{-2}	In ultrapure water, all the four pharmaceuticals were degraded by more than 95% within 4 min, the same removal rate expended about 30–60 min. Except for DF, the cytotoxicity increase during the degradation process for SP, SMX and SIM.	[72]

SMZ	Photoelectro-chemical	[SMZ] = 10 mg L^{-1} pH = 3.5 Potential = 2 V	The removal efficiency of SMZ by photoelectrochemical process was 81.3%, which was approximately twice the sum of both electrochemical and photochemical processes, and over 40% of TOC was eliminated after 180 min.	[73]
SD	Photocatalysis	[SD] = 10 mg L^{-1} pH = 8	Nearly 70% of SD was degraded by the $Ag_3PO_4/MoS_2/TiO_2$ NTAs in 240 min, which was higher than that of MoS_2/TiO_2 (35%) and Ag_3PO_4/TiO_2 NTAs (44%). In addition, the percentage of SD removal over direct photolysis, electrochemical and photochemical was only 16, 20 and 31%, respectively.	[74]
SP	US-CN	pH = 7.5 [SP] = 0.03 mmol L^{-1} catalyst dosage = 32 mg UV intensity = 100 mW cm^{-2}	The time-dependent removal efficiency of SP over different carbon nitride samples was 90.55%, 50.77% and 26.19% of SP by US-CN, S-CN and CN after 100 min of photocatalytic reaction. The removal rates of SP at 100 min in river water (Shanghai), pharmaceutical water (Guangzhou), domestic wastewater (Guangzhou) and tap water (laboratory) reached up to 84.74, 75.66, 82.06 and 85.26%, respectively.	[75]
AMX	UV/H_2O_2 and UV/persulfate	[AMX] = 20 μmol L^{-1} [H2O2] = [PS] = 500 μmol L^{-1}	The direct UV photolysis system alone showed an insignificant AMX degradation. However, the addition of H_2O_2 or PS increases the degradation efficiency of AMX significantly. Despite the high percentage of AMX removal through UV/AOPs, the mineralization of AMX was insignificant. After 30 min of treatment, only 15.2% and 28.7% of TOC were removed in the UV/H_2O_2 and UV/persulfate systems, respectively.	[76]
AMX	Fenton process, photo-Fenton, solar photo-Fenton, sono-Fenton, and sono-photo-Fenton	pH = 3 [AMX] = 10 mg L^{-1} [$FeSO_4$] = 3.0 mg L^{-1} [H_2O_2] = 375 mg L^{-1} Ultrasound = 40 kHz, Light source = UV tubes 365 nm	Under the optimized conditions, Fenton's process was able to remove 100% of AMX within 12 min of reaction time. Coupling the Fenton process with UV-light illumination, solar light illumination and UV light–ultrasound treatment allowed complete antibiotic removal in 3.5, 9 and 6 min, respectively.	[77]
AMX	solar photo-Fenton	[Fe^{3+}] = 3 mg L^{-1} [H_2O_2] = 2.75 mg L^{-1} [AMX] = 1 mg L^{-1}	A total of 94 and 66% of AMX was removed after 60 and 210 min of treatment in simulated and real wastewater, respectively. In addition, the percentage of TOC removal for AMX was 19.5% in simulated wastewater. In the study carried out with real effluent, the removal rate was 6.5%.	[47]
AMX	Photolysis	[AMX] = 20 mg L^{-1} pH = 7 catalyst dosage = 0.5 g L^{-1}	Photolysis under the simulated sunlight was ineffective in the decomposition of AMX, while pure V_2O_5 and C_3N_4 reached 33.2%	[48]

			and 52.7% of AMX removal under 120 min illumination. The V_2O_5/C_3N_4 (1 wt% V_2O_5) nanocomposite increased AMX removal to 91.3%. Moreover, 1-V_2O_5/C_3N_4 nanocomposite attained 76.2% of TOC removal under the same conditions.	
CP	solar photoelectro-Fenton	[CP] = 0.230 mmol L^{-1} pH = 3 j = 50 mA cm^{-2} [Fe^{2+}] = 0.50 mmol L^{-1}	At the best conditions, the degradation of CP by SPEF reached 100% removal in only 15 min, while using EF, a complete removal was achieved in about 20 min. The AO-H_2O_2 process was capable of removing only 36% in 30 min of treatment.	[51]

Abbreviations: CP: captopril; AMX: amoxilin; SMZ: sulfamethazine; SDZ: sulfadiazine; SML: sulfamethizole; DF: diclofenac; SP: sulpiride; SMX: sulfamethoxazole; SIM: sulfisomidine; SD: sulfadiazine; VEN: venlafaxine; SFX: sulfamethoxazole; FLU: fluoxetine; CBZ: carbamazepine.

3.4. Sulfurized-Based Compounds

Sulfonamides (SA) are widely used as antibiotics in human and veterinary medicine due to their high antimicrobial activity, stable chemical properties and low costs [69,78]. SA has been found in surface waters at concentrations of 148–2978 ng L^{-1} [69]. Therefore, Moradi and Moussavi [70] investigated the degradation, mineralization and mechanism of sulfamethoxazole (SMX) oxidation in a UVC/VUV reactor. Total SMX (100 mg L^{-1}) removal was reached in pH 7 and at a fluence of 54.9 mJ cm^{-2}, while the TOC removal of 98.5% was obtained at fluence of 109.8 mJ cm^{-2}. In addition, mineralization was also evaluated by measuring the concentrations of nitrate, ammonium and sulfate ions. The nitrogen and sulfur releases of 83.44% and 96.58%, respectively, during the SMX degradation confirmed high mineralization. Scavenging tests using alcoholic radicals scavengers and salicylic acid proved that OH was the dominant radicals specie involved in the degradation of SMX.

Acosta-Rangel et al. [69] conducted an interesting study on the degradation of three SAs, sulfamethazine (SMZ), sulfadiazine (SDZ) and sulfamethizole (SML), by UV, UV/H_2O_2 and UV/$K_2S_2O_8$. Based on the quantification of the UVC radiation, the low values of quantum yield at 60 min of treatment were observed. According to the authors, the UVC dose commonly applied for water disinfection (400 J m^{-2}) in treatment plants proved inadequate to remove these compounds, requiring higher UV radiation doses or longer exposure times. Directing the UVC photolysis of SAs is influenced by their initial concentration (5, 10 and 15 mg L^{-1}), the degradation rates were higher at pH 12 due to the SAs are in their anionic form for SMZ and SML (Figure 6a). A concentration of 4.4×10^{-4} mol L^{-1} of H_2O_2 or $K_2S_2O_8$ increases SMZ degradation by up to 100%. UVC/PDS costs less energy than UVC and UVC/H_2O_2.

According to Figure 6b, SO_2 removal is first produced by direct SMZ photolysis through UVC radiation, obtaining by-product P1. Next, given the oxidation of OH· radical during the process, hydroxylation is expected to be a common reaction responsible for SMZ degradation, generating by-products P3-1, P3-2, P5-1 or P5-2. A break in the $-SO_2-$ and −NH− bond allows the identification of the by-product P2. By attacking nucleophilic and incision in the group $-SO_2-$, the byproduct P4 may be formed. While the adduction of seven N atoms, forming the nitroso- and nitro-substitutional SMZ through the electrophilic reaction was the dominant pathway by PDS (P6 and P7). Moreover, cytotoxicity tests revealed that the by-products formed were less toxic than the original products.

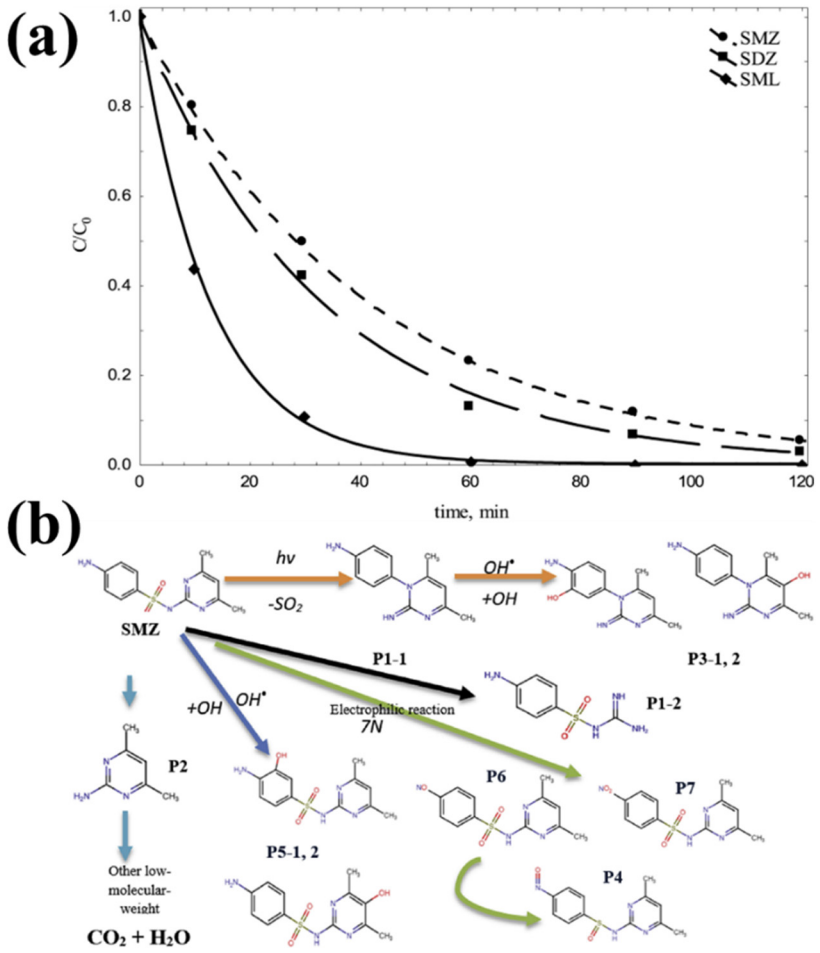

Figure 6. (**a**) Degradation kinetics of the three SAs by UVC photolysis. $[SAs]_0$ = 15 mg L^{-1}, pH = 7 and T = 298 K. The lines represent the prediction of the first-order kinetic model. (**b**) Mechanism of degradation by direct SMZ photolysis in the presence of UVC radiation. Reprinted with permission from [69]. Copyright © 2023 Elsevier Ltd.

Similar behavior was observed by Lin and Wu [79] and Wen et al. [71] when investigating the degradation of sulfamethazine (SMT) in an aqueous solution by the UV/H_2O_2 and VUV/UV photo-Fenton processes, respectively. Li and Wu [79] reported that SMT (10 mg L^{-1}) was 100% degraded in half the time (15 min) after adding 10 mmol L^{-1} of H_2O_2, while the UV process degraded 79% of the SMT after 30 min. Wen et al. [71] evaluated the mineralization of SMT ($[SMT]_0 = 1.8 \times 10^{-2}$ mmol L^{-1}, $[H_2O_2]_0 = 0.74$ mmol L^{-1}, $[Fe^{3+}]_0 = 0.25$ mmol L^{-1}, $pH_0 = 4.0$) and found that it was significantly enhanced in the VUV/UV photo-Fenton process as compared to the UV and UV photo-Fenton processes after 60 min of treatment, achieving ~60% of TOC removal. The authors also reported the effect of the initial concentration of SMN on the reaction mechanism. At low concentrations of SMN (1.8 μmol L^{-1}), indirect oxidation is primarily responsible for the degradation of SMN; while at higher concentrations (90 μmol L^{-1}), both photolysis and indirect oxidation contributed to the degradation of the compound.

More recently, Hong, Wang and Lu [72] reported the degradation of a complex matrix of four common refractory pharmaceuticals, diclofenac (DF), sulpiride (SP), sulfamethoxazole (SMX) and sulfisomidine (SIM) present in a disc tubular reverse osmosis (DTRO) concentrator from the local landfill by UV-Fenton system. In the ultrapure water, all four pharmaceuticals were degraded by more than 95% within 4 min, while in the DTRO concentrates, the same removal rate expended by about 30–60 min under the same dosage of H_2O_2 (100 times of the $[pharmaceuticals]_0$ = 20 mg L^{-1}), catalyst (1/200 mol L^{-1} of

$FeSO_4 \cdot 7H_2O$ and H_2O_2) and UV intensity (λ = 253.7, 75 mW cm^{-2}). A total of 49 transformation products (TP) were identified by HPLC-MS, and 22 new TPs were first found and presented. Toxicity evolutions on HepG2 cells during UV–Fenton treatment revealed that, except for DF, the cytotoxicity increased during the degradation process for SP, SMX and SIM.

The degradation of sulfonamides was also performed by employing photoelectrochemical semiconductors. Jia and co-workers [73] obtained visible light-driven semiconductor-metal organic frameworks (MOFs), which were constructed by electro-anodization and the deposition growth method. ZIF-8 (zeolitic imidazolate framework) nanoparticles were deposited on the hollow TiO_2 nanotubes and N and F were added as co-doping and the electrode as nominated ZIF-8/NF-TiO_2. The removal efficiency of SMZ (10 mg L^{-1}) through the photoelectrochemical process was 81.3%, which was approximately twice the sum of both electrochemical and photochemical processes, and over 40% of TOC was eliminated after 180 min, suggesting that SMZ could be partially mineralized by ZIF-8/NF-TiO_2 under visible light irradiation. The degradation pathway of SMZ was divided into three steps: cleaving, aromatic ring opening and mineralizing.

In another study, Teng et al. [74] reported the decomposition of sulfadiazine (SD) by $Ag_3PO_4/MoS_2/TiO_2$ nanotube array (NTAs) electrode, under visible light excitation. TiO_2 NTAs were modified with MoS_2 nanosheets and Ag_3PO_4 nanoparticles through photo-assisted electrochemical deposition and chemical immersion methods. Nearly 70% of SD was degraded by the $Ag_3PO_4/MoS_2/TiO_2$ NTAs in 240 min, which was higher than that of MoS_2/TiO_2 (35%) and Ag_3PO_4/TiO_2 NTAs (44%). In addition, the percentage of SD removal over direct photolysis, electrochemical and photochemical was only 16, 20 and 31%, respectively. The results demonstrating that the Ag_3PO_4 nanoparticles increased the visible light absorption and MoS_2 nanosheet promoted the separation of photogenerated charges effectively.

Ultrathin S-doped graphitic carbon nitride nanosheets (US-CN) were synthesized and its SP removal efficiency was evaluated under various conditions via the visible-light-assisted peroxydisulfate (PDS-VL) activation method by She et al. [75]. The time-dependent removal efficiency of SP over different carbon nitride samples was 90.55%, 50.77% and 26.19% of SP by US-CN, S-CN and CN, respectively, after 100 min of photocatalytic reaction. The $^1O_2$ generated from US-CN/PDS-VL system was the major reactive oxidation species (ROS) for SP degradation. Three possible degradation pathways were proposed, combining theoretical studies and LC-MS. Pathway I included the attack on 9N atom with the C-N bond cleavage, followed by consecutives C-C bond cleavage. In pathway II, the C-N bond cleavage occurred through the attack on 12N atom, followed by SO_2 extrusion. While the attack on nine N atoms and SO_2 extrusion was ascribed as pathway III.

Later, the US-CN/PDS-VL system in SP degradation was applied in actual wastewater. The removal rates of SP at 100 min in river water, pharmaceutical water, domestic wastewater and tap water reached up to 84.74, 75.66, 82,06 and 85.26%, respectively, indicating a slight decrease compared with that in ultrapure water matrix, demonstrating the potential application of this system [75].

Amoxicillin (AMX) belongs to the β-lactams family and is often used for the treatment of bacterial infections, such as pneumonia and urinary tract infections [43]. It has been shown that over 80% of AMX is excreted through urine from the human body after 2 h of ingestion. This relatively fast egestion coupled with its extensive use has been attributed to AMX being one of the most widely reported antibiotics in wastewater, generating antibiotic-resistant bacteria and requires effective treatment methods [80–82].

Taking this into account, Zhang et al. [76] compared the reaction kinetics, degradation pathways and antibacterial activity of AMX in the UV/H_2O_2 and UV/persulfate systems. Direct UV (λ = 254 nm) photolysis system alone showed an insignificant AMX degradation (20 μmol L^{-1}), which was attributed to its low quantum yield of 9.74×10^{-3} mol E^{-1}. However, the addition of H_2O_2 or PS (500 μmol L^{-1}) increases the degradation efficiency of AMX significantly due to the generation of HO· and SO_4^{-}·. Despite the high

percentage of AMX removal through UV/AOPs, the mineralization of AMX was insignificant. After 30 min of treatment, only 15.2% and 28.7% of TOC were removed in the UV/H_2O_2 and UV/persulfate systems, respectively.

The by-products identified via LC/MSMS indicate three possible degradation pathways (Figure 7a), including hydroxylation, hydrolysis and decarboxylation. The intermediate with m/z of 382 indicates the mono-hydroxylation of AMX. HO·and SO_4^{-}·are expected to attack the sulfur atom on the thioether groups to yield sulfur centered radical cation by electron transfer. The radicals can be further deprotonated to generate α-thioether radicals, followed by oxidation to yield sulfoxide TP1, while HO· can attack the aromatic ring of the side chain to produce a hydroxyl radical, which can be further oxidized to form monohydroxy AMX TP2. Moreover, TP1 and TP2 can be hydroxylated to form the monohydroxy AMX sulfoxide TP3. The penicilloic acid, obtained by the hydrolysis by-product TP4, is formed by opening the strained four-membered beta-lactam ring of AMX. The decarboxylation product TP5 relates to the penicilloic acid derivative, generated by the subsequent release of the carboxyl group from the penicilloic acid. TP4 can also be hydroxylated at the sulfur atom and aromatic ring to generate TP6 and TP7, respectively. The products of AMX after UV/AOPs treatment possess significantly lower antibacterial activity. In addition, UV/H_2O_2 was more cost-effective than UV/PS process in the degrading AMX, according to the economic evaluation results [76].

The degradation of AMX has also been investigated using Fenton and coupled-Fenton processes. Verma and Haritash [83] studied the removal of amoxicillin using the Fenton process and hybrid Fenton-like processes, such as photo-Fenton, solar photo-Fenton, sono-Fenton and sono-photo-Fenton. Effects such as ferrous ions (Fe^{2+}), H_2O_2 and pH were evaluated. Under the optimized conditions of [Fe^{2+}] = 30 mg L^{-1}, [H_2O_2] = 375 mg L^{-1} and pH = 3, the Fenton process was able to remove 100% of AMX (10 mg L^{-1}) within 12 min of reaction time. Coupling the Fenton process with UV-light illumination, solar light illumination and UV light–ultrasound treatment allowed the complete antibiotic removal in 3.5, 9 and 6 min, respectively (Figure 7b). The authors concluded that the Fenton process coupled with other UV/solar light was more efficient than the stand-alone Fenton process for the degradation of AMX.

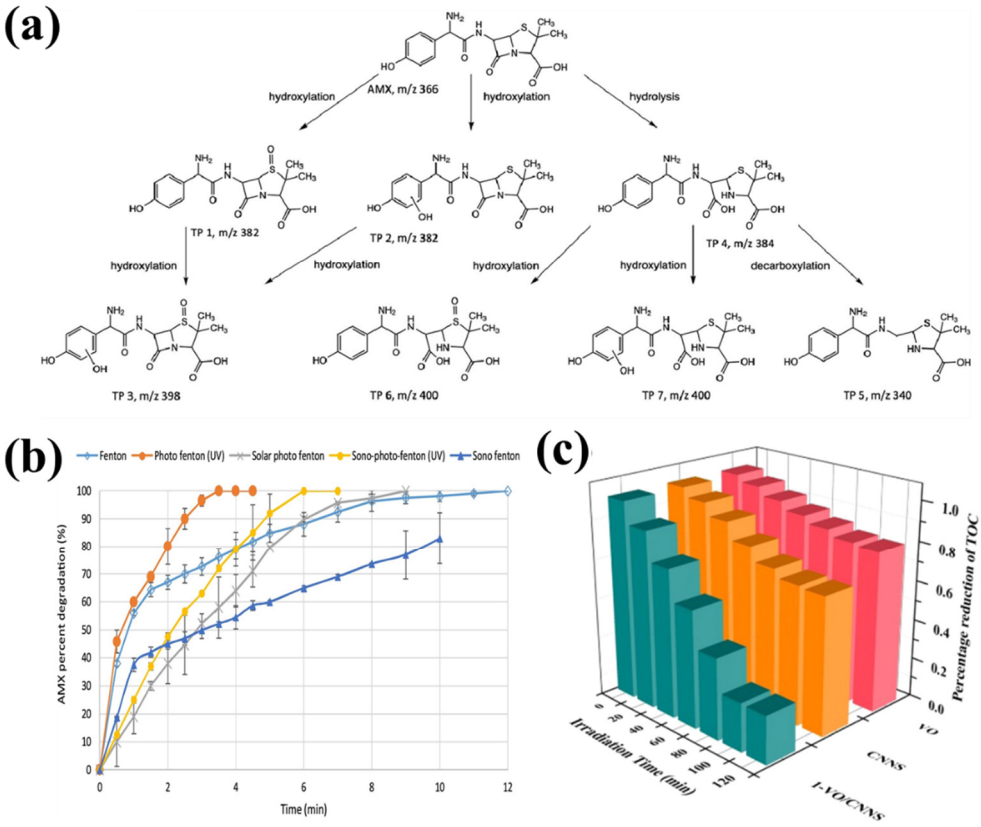

Figure 7. (**a**) Proposed pathway of AMX degradation. Reprinted with permission from [73]. Copyright © 2023 Elsevier Ltd. (**b**) Degradation of AMX at Comparison of Fenton, photo-Fenton, solar photo-Fenton, sono-Fenton and sono-photo-Fenton for complete degradation of AMX (AMX: 10 mg L^{-1}; $FeSO_4$: 3.0 mg L^{-1}; H_2O_2: 375 mg L^{-1}, pH: 3, Ultrasound: 40 kHz and light source: UV tubes (365 nm)). Reprinted with permission from [83]. Copyright © 2023 Elsevier Ltd. (**c**) TOC of AMX solution degraded under different irradiation time by as-prepared VO, CNNS and 1-VO/CNNS. Reprinted with permission from [84]. Copyright © 2023 Elsevier Ltd.

In another study, Guerra et al. [85] presented the results of the solar photo-Fenton oxidation of paracetamol (PCT) and amoxicillin in two aqueous matrices, a synthetic wastewater and real wastewater from El Ejido wastewater treatment plant effluent (Almeria). $Fe_2(SO_4)_3$ was used as the source of iron and ethylenediamine disuccinic acid (EDDS) as the iron complexing agent, employing different doses of H_2O_2. In all cases, the process was operated under conditions of natural sunlight. Amounts of 94 and 66% of AMX were removed after 60 and 210 min of treatment in simulated and real wastewater, respectively, using the optimized parameters: 3 mg L^{-1} Fe^{3+} and 2.75 mg L^{-1} H_2O_2. In addition, the percentage of TOC removal for AMX was 19.5% in simulated wastewater. In the study carried out with real effluent at concentrations of 2.75 mg L^{-1} H_2O_2, the removal rate was 6.5%, while at an H_2O_2 concentration of 5.0 mg L^{-1}, the removal rate increased to 20%. The intermediates identified suggest the hydroxylation of the aromatic ring and the opening of the four-membered β-lactam ring and subsequent formation of amoxilloic acid and amoxicilloic acid as the main transformation pathways.

Recently, Le and co-workers [85] reported an innovative heterostructure V_2O_5/C_3N_4 nanosheets (NS) photocatalyst to degrade AMX under solar light. Photolysis under the simulated sunlight was ineffective in the decomposition of AMX, while pure V_2O_5 and C_3N_4 reached 33.2% and 52.7% of AMX removal under 120 min of illumination. The 1-V_2O_5/C_3N_4-NS (1 wt% V_2O_5) nanocomposite increased AMX removal to 91.3%. This improvement was attributed to the enlarged specific surface area, increased active sites and promoted the separation of photoinduced electron–hole pairs by the S-scheme

heterojunctions. Moreover, 1-V_2O_5/C_3N_4-NS nanocomposite attained 76.2% of TOC removal under the same conditions (Figure 7c), showing the highest oxidation capacity. Furthermore, the authors confirmed that O_2^- and h^+ radicals are the foremost reactive species in photodegradation. Mmelesi et al. [86] also presented a high AMX removal percentage (89%) under visible light irradiation using $Zn_xCo_{1-x}Fe_2O_4$ (x = 0.0, 0.1, 0.2, 0.3, 0.4 and 0.5) nanoparticles. The catalysts were synthesized by a simple co-precipitation method. The Zn-doped NPs (x = 0.4) showed the highest degradation efficiency of 89% and TOC removal of 66.59% after 100 min.

Captopril is used as an antihypertensive in the treatment of heart failure, in cases of myocardial infarction, in diabetic nephropathy and as an angiotensin converting enzyme (ACE) inhibitor [87]. It is estimated that about 40 to 50% of the active ingredient is excreted from the human body and remains unchanged, while the rest is excreted as metabolites, which can be extremely dangerous for human health and must be evaluated against the contamination of surface waters due to the contamination of surface water due to incorrect disposal [88].

Dos Santos et al. [88] evaluated the electrochemical destruction of captopril in different aqueous matrices through the solar photo-electro-Fenton (SPEF) method using a solar pre-pilot flow plant with a Pt/air-diffusion cells and a planar photoreactor. The effect of j and drug content on the SPEF performance was studied, and comparative anodic oxidation (AO)-H_2O_2 and electro-Fenton (EF) assays were performed in order to confirm the superiority of SPEF process. At the best conditions (0.230 mmol L^{-1} of captopril, pH 3, j = 50 mA cm^{-2} and 0.50 mmol L^{-1} Fe^{2+}), the degradation of captopril by SPEF reached 100% of removal in only 15 min, while EF achieved complete drug removal in about 20 min. The AO-H_2O_2 process was capable of removing only 36% in 30 min of treatment. TOC was only reduced by 25% in SPEF after 300 min, suggesting that the resulting by-products were mainly oxidized by homogeneous OH, but contained very small amounts of Fe^{3+} complexes. The mineralization in urban wastewater (28%) was slightly accelerated as compared to those in sulfate medium because of the parallel oxidation with active chlorine. The drug removal was also feasible in urine, showing a larger mineralization of 70% [88].

Table 2 shows the main experimental conditions and results of the degradation and mineralization efficiency of the sulfurized-based drugs. In all studies presented, high degradation rates were achieved. In addition, UV alone proved ineffective in the removal of these compounds. However, it is worth noting that the authors used lamps to simulate radiation rather than sunlight to simulate light.

3.5. Phosphorus-Based Compounds

Ifosfamide (IF) and cyclophosphamide (CP) are two of the most used alkylating agents for the treatment of different cancers and autoimmune diseases that act directly on DNA, inhibiting cell division and, consequently, cell death [86–88]. Pharmacokinetic studies showed that 61% and 10–20% of the administered doses of IF and CP, respectively, are excreted unchanged via urine and feces, causing the emission of these drugs into the wastewater stream [89]. The metabolites and transformation products (TPs) residues of IF and CP have been found in the aquatic environment in amounts ranging from a few ng L^{-1} to tens of mg L^{-1}, indicating that these drugs are not readily biodegradable, making these compounds difficult to remove from wastewater by traditional methods [90].

Thus, Russo et al. [90] reported the IF and CP degradation by UV irradiation (λ = 254 nm) and investigated their acute and chronic ecotoxicity of and their commercially available human metabolites/TPs on different organisms of the aquatic trophic chain. After 48 h of treatment, IF and CP (200 mg L^{-1}) were degraded only 36.5% and 28.3%, respectively. According to the authors, this poor removal was attributed to the chemical structures of IF and CP that do not contain double bonds that could absorb photons under UV irradiation [89]. Moreover, DOC was monitored in UV irradiated samples containing IF and CP at 10 mg L^{-1} and revealed no significant decrease in DOC after 48 h of treatment,

suggesting that UV degradation was not able to mineralize both compounds. Regarding the toxicological tests, the UV-irradiated compounds showed an increase in toxicity. This effect was related to a mixture of different TPs formed during treatment.

In another study, Janssens et al. [91] coupled nanofiltration and UV, UV/TiO_2 and UV/H_2O_2 processes for the removal of anti-cancer drugs, which include CP and IF, from two different matrices: secondary wastewater effluent and nanofiltration concentrate. Direct photolysis was not able to remove IF and CP (500 μg L^{-1}) in secondary effluent after 180 min of treatment (Figure 8a), and the same behavior was reported in the work of Russo et al. [53]. The inefficiency of direct photolysis explains why IF and CP showed negligible removal through UV/TiO_2 (100 mg L^{-1}) and UV/H_2O_2 (40 mg L^{-1}): <25%. The same trend was observed during the degradation from nanofiltration retentate. CP and IF showed no degradation either through UV/TiO_2 or through UV/H_2O_2.

In an effort to increase the efficiency of the UVC/H_2O_2 system for the degradation of cyclophosphamide, Graumans et al. [92] coupled thermal plasma activation with UV-C/H_2O_2 treatment. Plasma-activated water (PAW) contains highly reactive oxygen and nitrogen species because of electric gas discharges in the air over water. The oxidative degradation of CP solutions (4 ng mL^{-1}) in tap water by PAW resulted in a complete degradation within 80 min at 150 W (Figure 8a). CP was also completely degraded within 60 min of applying the UVC/H_2O_2 (10 mg L^{-1}) system. In addition, LC-MS/MS detected the reaction products 4-keto-CP, 4-hydroperoxy-CP and carboxyphosphamide. Furthermore, the authors analyzed the implications of the toxicity of the products formed and highlighted the concern regarding the 4-Hydroperoxy-CP formation, a very potent toxic compound capable of alkylating DNA strands.

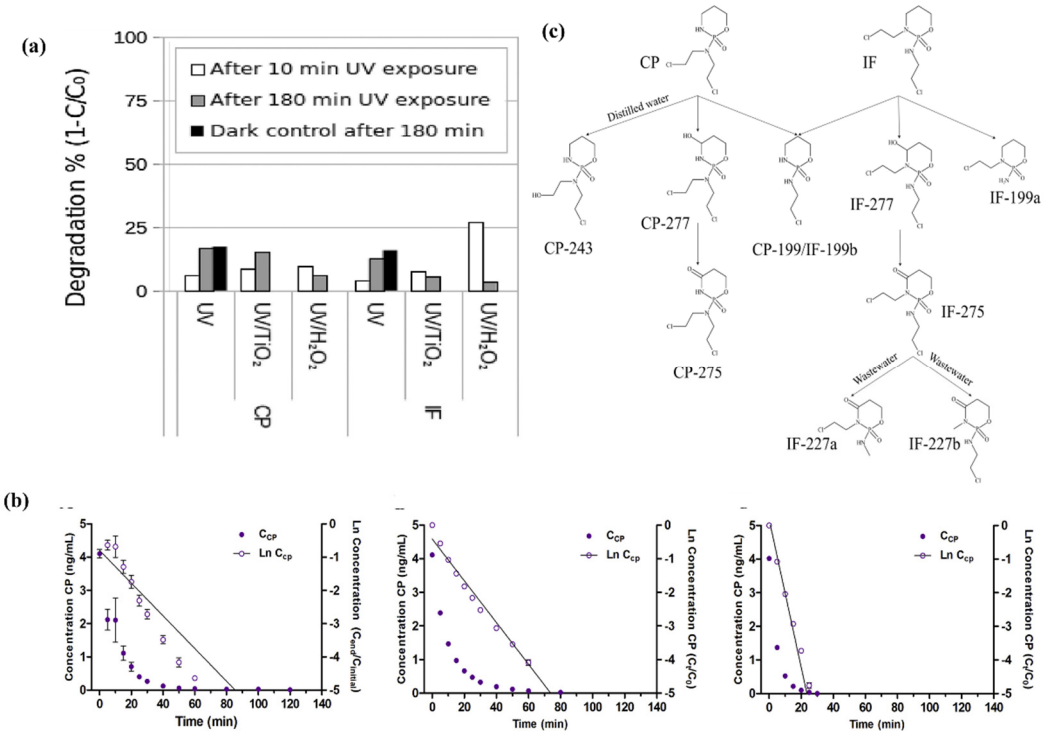

Figure 8. (**a**) Removal of cyclophosphamide (CP) and ifosfamide (IF) from a NF concentrate by UV, UV/TiO_2 (100 mg L^{-1}) and UV/H_2O_2 (40 mg L^{-1}). Reprinted with permission from [88]. Copyright © 2023 Elsevier Ltd. (**b**) Degradation rate of 4 ng mL^{-1} CP applied on TS1 in water at different hydrogen peroxide concentrations in combination with an UV-C source. With UV-C/H_2O_2 (970 mM) treatment, no complete CP removal was obtained within 120 min (left), in contrast with H_2O_2 concentrations 0.11 (center) or 0.22 mM (right), which showed complete and rapid CP removal rates. Reprinted with permission from [93]. Copyright © 2023 Elsevier Ltd. (**c**) Proposed photodegradation pathways for IF and CP. Reprinted with permission from [86]. Copyright © 2023 Elsevier Ltd.

Osawa et al. [89] investigated the photodegradation of CP and IF (10 mg L^{-1}) using ruthenium-doped titanate nanowires (Ru-TNW) in distilled water (DW) and wastewater (WW) from secondary wastewater treatment, under UV–Vis radiation. An improvement in the degradation of CP and If was observed using Ru-TNWas catalyst (20 mg), mainly when WW was used for solutions preparation. In addition, the results were better when the pollutants were used as single solutions. Using Ru-TNW as photocatalyst, the degradation of both compounds presented a higher removal rate independently on the matrix used and DW and WW from secondary treatment. CP and IF degradation experiments followed pseudo-first-order kinetics, and the degradation rate constant for IF was higher than the CP for both matrices.

Four CP transformation products (TPs) and six IF TPs from the photodegradation process were elucidated using high-resolution mass spectrometry (Figure 8c). The CP-277 was generated using the hydroxylation of CP while CP-275 was formed from the dehydrogenation of the hydroxy group connected with the heterocyclic ring from CP-277. According to the authors, CP-243 was formed by replacing the chlorine atom with the hydroxy group from the CP molecule. Moreover, it was considered that CP-199 was formed by the loss of the chloroethane group from CP and along with IF-199a and IF-199b are isomers. Additionally, IF-277 degraded to IF-275 through the dehydrogenation of the hydroxy group. In the WW samples, we believe that IF227a and IF-227b were generated from IF-275. For both pollutants, in the WW, there was a higher production of TPs and two of them were detected only in this matrix, indicating that environmental matrices may produce different TPs. Finally, the ecotoxicity prediction showed that TPs had low toxic potential on aquatic organisms. However, most of the TPs resulted in positive mutagenicity [89].

According to Table 4, it was possible to state that direct photolysis was not able to remove IF and CP. However, photo-combined AOPs systems showed elevated removal rates of the compounds. In addition, further studies may focus on mineralization or the formation of less toxic compounds, the importance of degradation intermediates should not be underestimated since the by-products generated using the systems presented in this work showed a toxicity that was the same or sometimes greater than the drug of origin.

Table 4. Selected recent studies of photo-assisted AOPs processes for phosphorus-based and oxygenated compound removal.

Pharmaceutical	Process	Experimental Conditions	Results	Ref.
IF and CP	Ru-TNW	[IF] = [CP] = 10 mg L^{-1} catalyst dosage = 20 mg pH = 7	The degradation of both compounds presented a higher removal rate independently to the matrix used; DW and WW in secondary treatment. CP and IF degradation experiments followed the pseudo-first-order kinetics and the degradation rate constant for IF was higher than the CP for both matrices.	[89]
IF and CP	UV irradiation	λ = 254 nm [IF] = [CP] = 10 mg L^{-1} pH = 7	After 48 h of treatment, IF and CP were degraded only by 36.5% and 28.3%, respectively, containing IF and CP at 10 mg L^{-1} and revealed no significant decrease in DOC after 48 h of treatment, suggesting that UV degradation was not able to mineralize both compounds.	[90]

IF and CP	UV irradiation, UV/TiO_2 and UV/H_2O_2	[IF] = [CP] = 500 μg L^{-1} [TiO_2] = 100 mg L^{-1} [H_2O_2] = 40 mg L^{-1} λ = 254 nm pH = 7	Direct photolysis was not able to remove IF and CP in secondary effluent after 180 min of treatment. CP and IF did not degrade negligibly either through UV/TiO_2 or through UV/H_2O_2.	[91]
CP	UVC/H_2O_2/PAW	λ = 254 nm [CP] = 4 ng mL^{-1} [H_2O_2] = 10 mg L^{-1} pH = 7	The oxidative degradation of CP solutions in tap water by PAW resulted in a complete degradation within 80 min at 150 W. CP was also completely degraded within 60 min applying UVC/H_2O_2 system.	[92]
IBP,NPX and MO	MIL-53(Al)@TiO_2 and MIL-53(Al)/ZnO	[compound] = 6 mg L^{-1} pH = 6.8 catalyst dosage = 2 mg	MIL-53(Al)@TiO_2 exhibited high photodegradation efficiency (80.3%) for NPX over 4 h and was recyclable for up to three cycles with only a 13.6% decrease in photodegradability. However, for IBP degradation, MIL-53(Al)@ZnO was observed to be more efficient than MIL-53(Al)@TiO_2 and it was found that only 1 h of treatment was sufficient to obtain a considerable COD reduction of 58%.	[93]
NPX	UV irradiation, UV/chorine and UV/H_2O_2	[NPX] = 5 μmol L^{-1} [chlorine] = [H_2O_2] = 50 μmol L^{-1} λ = 254 nm pH = 7	NPX was degraded by 27.3% at a UV dosage of 922 mJ cm^{-2}. The degradation of NPX by both AOPs followed pseudo-first-order kinetics, and the first-order rate constant was 4.9 times higher in UV/chlorine than that in UV/H_2O_2.	[94]
IBP, NPX and CTZ	PAN-MWCNT/TiO_2–NH_2	[compound] = 5 mg L^{-1} pH = 2 UV intensity = 40 W catalyst dosage = 15 mg	The complete degradation of IBP required 120 min of treatment, while the same degradation rate for NPX was achieved in 40 min.	[95]
KET	UV irradiation	UV intensity = 1700 μW cm^{-2} [KET] = 16 mg L^{-1} pH = 7	The maximum removal rate of KET reached 99.59% within 40 min, which agrees with the pseudo-first-order kinetic equations.	[96]
KET	CuO/TiO_2@GCN	[KET] = 10 mg L^{-1} pH = 6.2 (GW) and 7.4 (DW) catalyst dosage = 75 mg	At the best conditions, the impregnation of 1% CuO/TiO_2 into GCN presented an efficiency of 94.7% in the photodegradation of KET in deionized water under simulated light. A lower removal efficiency (~50%) was achieved in ground (GW) and drinking water (DW).	[97]
IBP	Ag-Ce/TiO_2 (Co-DPU) and Ag-Ce/TiO_2 (C-IMP)	Visible light = 239 W m^{-2} λ > 400 nm catalyst dosage = 0.1 g L^{-1} [IBP] = 10 mg L^{-1} pH = 5.3–5.6	The obtained TOC conversion followed the decreasing order: Ag-Ce/TiO_2 (Co-DPU) > Ag-Ce/TiO_2 (C-IMP) >TiO_2. After 4 h, up to 98% mineralization of IBP was obtained for Ag-Ce/TiO_2 (Co-DPU).	[98]
IBP	UV/H_2O_2	[IBP] = 10 μmol L^{-1} [H_2O_2] = 0.5 mmol L^{-1} pH = 7–7.5	IBP was degraded by 8 and 3% under UV and H_2O_2 only, while the combined	[99]

		λ = 254 nm	UV/H_2O_2 process removed 78% of IBP within 4 min.	
ASA	Photo-Fenton	[ASA] = 10 μg L^{-1} [Fe^{2+}] = 1.5 mmol L^{-1} [H_2O_2] = 45 mmol L^{-1} UV intensity = 40 W pH = 7	Using optimized conditions, 90% of mineralization was reached in 10 min.	[100]
ASA	UV/O_3	[ASA] = 10 mg L^{-1} [O_3] = 2.4 mg L^{-1} UV intensity = 2600 μW cm^{-2} pH = 4.3	The UV/O_3 process was able to remove 99% of ASA after 7 min of treatment. Moreover, the combined process exhibited higher mineralization rate, 47% of TOC reduction, compared with the individual ozonation process (25% of TOC) after 30 min.	[101]
ASA	UV/ZnO	UV Intensity = 6 W catalyst dosage = 375.16 mg L^{-1} [IBP] = 33.84 mg L^{-1} pH = 5.05	At the optimized conditions, the ASA removal of 83.11% was achieved. The kinetic studies showed that the pseudo-first-order model had the highest correlation with aspirin removal using the UV/ZnO photocatalytic process.	[102]
ASA	1-Ni-MnON/NG	[ASA] = 75 mg L^{-1} catalyst dose = 10 mg L^{-1} pH = 3 UV Intensity = 4.2 W	Almost complete degradation was achieved for the nanocomposites of 1-Ni-MnON/NG after 90 min of treatment.	[103]

Abbreviation: ifosfamide (IF); naproxen (NPX), methyl orange (MO); naproxen (NPX); cetirizine (CTZ); ketoprofen (KET); aspirin (ASA).

3.6. Oxygenated-Based Compounds

Ibuprofen (IBP), naproxen (NPX) and ketoprofen (KET) are non-steroidal anti-inflammatory drugs (NSAIDs), one of the pharmaceuticals groups widely detected in the environment. IBP and NPX are most used for the treatment of musculoskeletal injuries, rheumatoid arthritis and fever [93,104]. Several studies have detected these compounds in surface water and groundwater and even in drinking water sources at several concentrations due to the limited removal efficiency during the municipal sewage treatment processes [93].

In this sense, Pan et al. [104] compared the kinetics and pathways of the degradation of NPX by the UV/chorine and UV/H_2O_2 processes. NPX (5 μmol L^{-1}) was degraded by 27.3% at a UV dosage of 922 mJ cm^{-2} due to the high molar absorptivity at 254 nm of 4024 M^{-1} cm^{-1}. However, the degradation of chlorine or H_2O_2 alone was negligible. The degradation of NPX by both AOPs followed pseudo-first-order kinetics, and, at pH 7, the first-order rate constant (k′) was 4.9 times higher in UV/chlorine than that in UV/H_2O_2 ([chlorine]$_0$ = [H_2O_2]$_0$ = 50 μmol L^{-1}). Evaluating the relative radicals contribution, radicals chlorine species, such as Cl·, ClO· and Cl_2^{-}, are dominant in the NPX degradation through UV/chlorine while HO· played a dominant role during the NPX removal by UV/H_2O_2. The degradation by both AOPs was associated with hydroxylation and demethylation; in particular, decarboxylation was observed in UV/H_2O_2, and chlorine substitution was observed in the UV/chlorine process. The acute toxicity of *Vibrio fischeri* in UV/chlorine was lower than that of the system using only UV radiation, besides following an increase and then decrease trend with increasing reaction times, which was related to the production of different compounds during the reaction.

In another study, Mohamed and co-workers [95] reported the photodegradation of ibuprofen, naproxen, and cetirizine in aqueous media under UV irradiation. The

photocatalyst consisted of TiO_2-NH_2 nanoparticles grafted into polyacrylonitrile (PAN)/multi-walled carbon nanotube composite nanofibers (PAN−CNT). The authors investigated the effect of pharmaceutical initial concentration (5−50 mg L^{-1}), solution pH (2−9) and irradiation time on degradation efficiency. It was shown that the complete degradation was achieved at low drug concentration (5 mg L^{-1}), pH = 2, at a low power intensity of the UV lamp (40 W) and employing a dosage of 15 mg of PAN-MWCNT/TiO_2–NH_2 photocatalyst. In addition, the complete degradation of IBP required 120 min of treatment, while the same degradation rate for NPX was achieved in 40 min.

Zhen, Liu and Zhang [96] studied the removal effect of KET in UV-light and explored the influence of light turbidity, light intensity and other factors on the degradation efficiency of ketoprofen. The results show that deep ultraviolet treatment has a good degradation effect on ketoprofen. After irradiation with 1700 μW cm^{-2} UV lamps, the maximum removal rate of KET (16 mg L^{-1}) reached 99.59% within 40 min, which agrees with the pseudo-first-order kinetic equations. In addition, the irradiation strength of UV lamps showed little influence on KET degradation. Moreover, low turbidity (1-5NTU) solutions reduced the degradation rate of ketoprofen, while high turbidity (5-9NTU) solutions enhanced the removal rate of ketoprofen.

Murtaza et al. [93] reported the photodegradation studies of single and binary mixtures of naproxen, ibuprofen and methyl orange, employing photocatalysts prepared by incorporating TiO_2 and ZnO into the framework of the aluminum-based MOF (metal organic frameworks), MIL-53(Al) (MIL = Materials from the Lavoisier Institute), MIL-53(Al)@TiO_2 and MIL-53(Al)/ZnO. MIL-53(Al)@TiO_2 exhibited high photodegradation efficiency (80.3%) for NPX over 4 h and was recyclable for up to three cycles with only a 13.6% decrease in photodegradability. A ratio of 3:1 concentration of NPX to mass of photocatalyst was found to be optimum for degradation. However, for IBP degradation, MIL-53(Al)@ZnO was observed to be more efficient than MIL-53(Al)@TiO_2. Experiments conducted with scavengers showed that hydroxyl radicals played a major role in the photocatalytic process photodegradation, and it was found that only 1 h of treatment was sufficient to obtain a considerable COD reduction of 58%.

Mofokeng et al. [97] studied the formation of CuO/TiO_2@GCN (graphitic carbon nitride) and its applicability to the decomposition of KET in an aqueous environment, drinking water, and groundwater under simulated visible light. At the best conditions, the impregnation of 1% CuO/TiO_2 into GCN presented an efficiency of 94.7% in the photodegradation of KET (10 mg L^{-1}) in deionized water under simulated light. A lower removal efficiency (~50%) was achieved in ground and drinking water due to electrical current and high conductivities of the water samples. In addition, the photocatalytic degradation of KET followed the pseudo-first-order kinetics and the rate constants in ground and drinking water were slower compared to deionized water (Figure 9a). The authors justified that the ground and drinking water contains substances that could have interfered with the catalysts active sites and inhibit its catalytic activities. The electrical energy consumption (E_{EC}) utilized for KET photodegradation in ground and drinking water was 5.9 and 7.0 times higher than the E_{EC} used in deionized water. LC/MS coupled with a Q-TOF analyzer indicated that the KET degradation entailed the deprotonation of the carboxyl group, followed by decarboxylation forming KET intermediates, which included benzylic and ketyl radical structures.

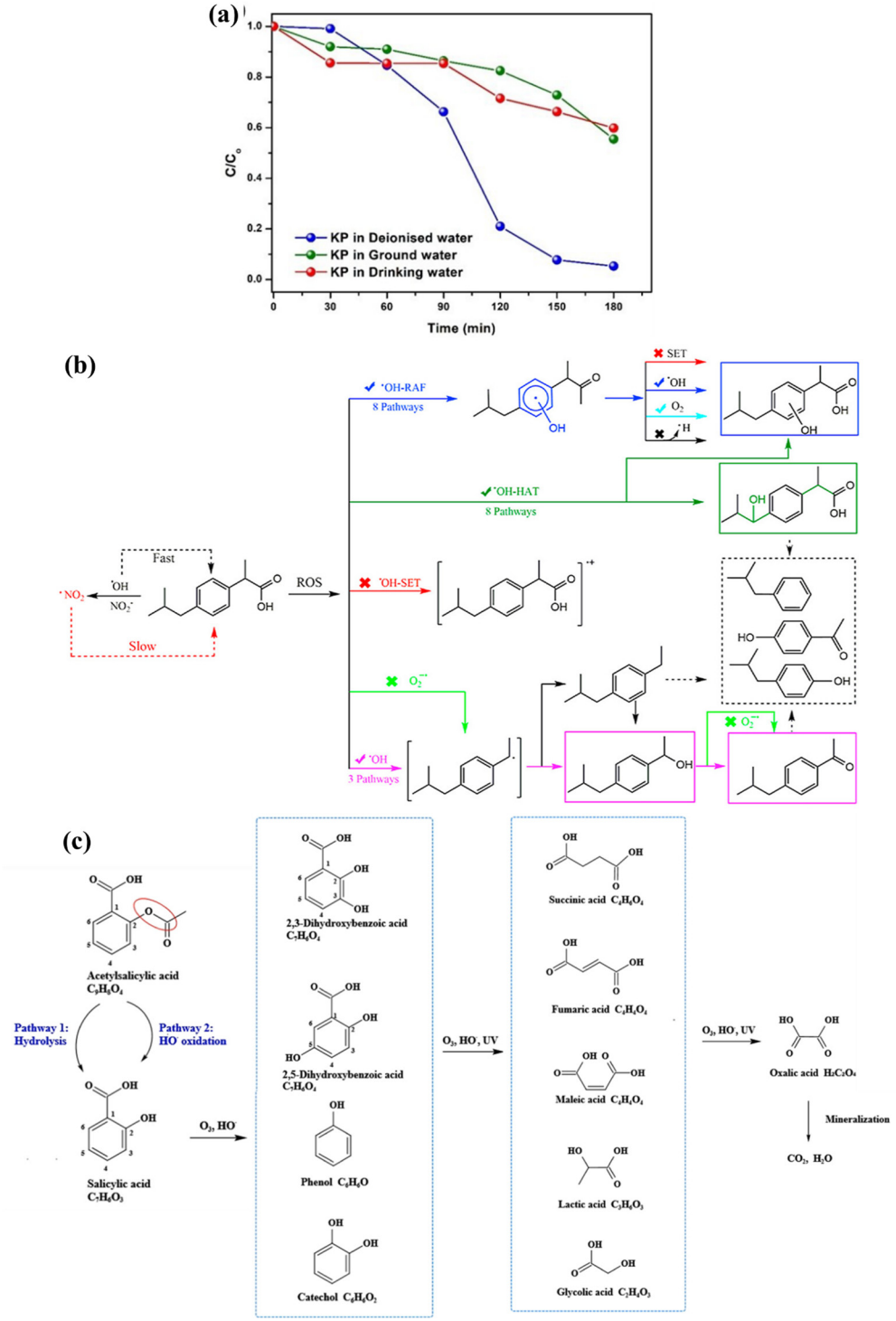

Figure 9. (**a**) Photocatalytic degradation of KP in deionized drinking and ground water using 75 mg of 1% CuO/TiO2@GCN (9:1). Reprinted with permission from [97]. Copyright © 2023 John Wiley and Sons. (**b**) Proposed degradation pathways for IBP. Reprinted with permission from [99]. Copyright © 2023 Elsevier Ltd. (**c**) Reaction pathway of ASA during UV/O3 process. Reprinted with permission from [101]. Copyright © 2023 Elsevier Ltd.

The degradation of IBP under visible light irradiation was also investigated by Chaker, Fourmentin, and Chérif-Aouali [98] using TiO_2 mesoporous co-doped with Ag and Ce. The co-doped photocatalysis was obtained using two different methods: co-impregnation (Co-IMP) and co-deposition precipitation with urea (Co-DPU). The obtained TOC conversion followed a decreasing order: Ag-Ce/TiO_2 (Co-DPU) > Ag-Ce/TiO_2 (C-

IMP) > TiO_2. After 4 h, up to 98% mineralization of IBP was obtained for Ag-Ce/TiO_2 (Co-DPU). Additionally, the stability of Ag-Ce/TiO_2 (Co-DPU) was evaluated during three cycles of use and reuse. TOC removal remained unchanged, ranging from 97 to 98% after three cycles. Later, the authors identified the products for IBP mineralization and found that through the hydroxylation process by the attack of·OH radicals, IBP may be transformed into hydroxy ibuprofen. The reaction follows until the ring opening for the total mineralization, leading to the formation of CO_2 and H_2O.

Wang et al. [99] investigated the degradation kinetic and transformation mechanism of IBP in UV/H_2O_2 process. Impacts of H_2O_2 dosage, pH, quenching agent and concentration of nitrite (NO_2^-) on IBP degradation were evaluated. IBP (10 μmol L^{-1}) was degraded by 8 and 3% under UV and H_2O_2 only, while the combined UV/H_2O_2 ([H_2O_2] = 0.5 mmol L^{-1}) process removed 78% of IBP within 4 min. At higher concentrations of H_2O_2, the IBP degradation became slower, which was attributed to the production of the radicals of low oxidation ability (HO_2 or O_2^-). Regarding the impact of pH, the degradation of IBP decreased with the pH increases from 5.2 to 9.6. The phenomenon was explained by the formation of scavenger species and the photolyzation of H_2O_2 into water and oxygen under alkaline conditions (Figure 9b).

Moreover, the addition of different concentrations of NO_2^- had a significant inhibitory effect on the degradation of IBP. According to the authors, nitrites reacted with ·HO to produce NO_2, which exhibited lower reactivity to compounds with electron-withdrawing moieties [105]. Combining ultra-high-resolution mass and density functional theory calculations, the authors identified hydroxylation as the first step in IBP degradation (Figure 9b) in indirect photolysis, as observed in another papers [98], and the formation of decarboxylation products (1-(4-isobutylphenyl) ethanol and 4-isobutylacetophenone), and some of the products of subsequent degradation of 4-IBP [99].

Aspirin (acetylsalicylic acid: ASA) also belongs to the NSAIDs group and is widely used for pain, infection or inflammation. ASA as a pollutant is found with a different concentration, from 0.03 to 10 μg L^{-1}, in aqueous environment and found to be very toxic for human health and the aquatic system due to a short half-life of 2–3h, and therefore, its removal from the environment is important [100,106]. Thus, Cunha-Filho et al. [100] optimized the kinetic conditions to mineralize ASA using a photo-Fenton process with UVA radiation in a tubular photochemical reactor. Employing a statical tool-termed factorial design, a large interval of concentrations of ASA, Fe^{2+} and H_2O_2 were studied. Using the optimized conditions of H_2O_2 and Fe^{2+} (45 and 1.5 mmol L^{-1}, respectively), 90% of mineralization was reached in 10 min. Such performance was attributed to the optimized 4.5-folds excess of [H_2O_2], i.e., the ratio of the stoichiometric [H_2O_2] to the theoretic TOC for total mineralization.

In another study, Zhe and co-workers [101] investigated the removal of ASA through the UV/O_3 process. The initial reaction positions and the byproducts were also identified. The UV/O_3 process was able to remove 99% of ASA (10 mg L^{-1}) after 7 min of treatment. Moreover, the combined process exhibited higher mineralization rate, 47% of TOC reduction, compared with the individual ozonation process (25% of TOC) after 30 min. It was demonstrated, through the inhibition function of t-butanol addition, that ·HO made a significant contribution to the UV/O_3 process. The optimal values of pH were 4.3 and 10.0 for ASA removal and mineralization, respectively. Higher pH values lead to the decomposition of the ozone to produce ·HO species. These species have a stronger effect on the mineralization of organic compounds than O_3 molecules.

Frontier electron density (FED) analysis confirmed that the initial oxidation sites of HO· were located on the benzene ring of ASA, which generated salicylic acid (SA) more directly and enhanced SA transformation efficiency during the UV/O_3 process. An ASA degradation pathway was proposed and involved hydrolysis and hydroxylation reactions (Figure 9c), the opening of the benzene ring, the further oxidation of the alkyl chain byproducts and finally mineralization [101]. Pathway 1 included the hydrolysis of the ester group in ASA. In parallel, the C2 position could be attacked by HO·, resulting in the

hydroxyl substitution reaction, leading to the formation of SA (pathway 2). The ortho/para positions are more electron-rich due to the presence of hydroxyl groups (a strong electron donor). This makes the ortho and para positions of the benzene ring more susceptible to oxidant attacks with the generation of two hydroxylation byproducts, 2,3-dihydroxybenzoic acid and 2,5-dihydroxybenzoic acid (Figure 9c) Phenol was another aromatic byproduct, and its formation involved the decarboxylation of SA during HO· upon UV irradiation. The further hydroxylation of phenol was able to generate catechol, and the resulting aromatic byproducts were oxidized again. With the opening of the benzene ring, alkyl carboxylic acids containing two to four carbons were formed and were further degraded until the formation of oxalic acid, and after that, the mineralization occurred [101].

To optimize ASA removal from aqueous solution by the UV/ZnO photocatalytic process, Karimi, Baneshi and Malakootian [69] used response surface methodology (RSM) to study the influence of different parameters, such as ASA initial concentration (10−100 mg L^{-1}), ph (3−11), contact time (10−120 min) and ZnO catalyst dosage (100−600 mg L^{-1}). The optimized conditions included a pH solution of 5.05, after 90.5 min of treatment, employing a ZnO catalyst dosage of 375.16 mg L^{-1} and ASA initial concentration of 33.84 mg L^{-1} achieved the ASA removal of 83.11%. The effect of chloride and phosphate (20 mg L^{-1}) on the ASA degradation resulted in the increased removal efficiency (83.11% to 94.7%) and reduced the removal efficiency (from 83.11% to 56%), respectively. This behavior was attributed to the competition of the anion phosphate with the nanoparticles in ASA degradation for adsorption on the catalyst surface.

Mohan et al. [103] prepared Ni-decorated manganese oxynitride on graphene nanosheets for the degradation of ASA. Besides the effect of catalyst's composition, the authors examined the influence of other experimental parameters, such as initial concentration, catalyst dose, initial pH and additives. The best performance was achieved with the ASA initial concentration of 75 mg L^{-1}, with the catalyst dose of 10 mg L^{-1} and the initial pH 3. Almost complete degradation was achieved for the nanocomposites of 1-Ni-MnON/NG after 90 min of treatment. The detection of intermediates during photocatalysis showed that ASA undergoes hydroxylation, demethylation, aromatization, ring opening and finally complete mineralization into CO_2 and H_2O by reactive species. The catalyst remained stable even after five cycles of usage, proving its reusability. Cytotoxicity, plant toxicity and microbial toxicity studies corroborate the environmentally friendly properties of the synthesized material.

In this sense, photo-combined systems have shown promise in the removal and mineralization of oxygen-based compounds (Table 4).

4. Conclusions and Outlook

This review has showed the prospective application of photo- and photo-combined AOPs for the removal of pharmaceuticals compounds. Current research demonstrates that pharmaceuticals have been found in distinct kinds of surface waters, wastewaters and WWTP and hospital effluents. Furthermore, the presence of these compounds in water may have harmful effects on human beings as well as promote the spread of resistant bacterial strains.

Several studies have applied photo- and photo-combined AOPs to removing pharmaceuticals in water or wastewater. Overall, the works presented here discussed (I) degradation kinetics by investigating the effect of operational parameters; (II) mineralization measurements using indicators, such as TOC, DOC or COD; (III) toxicity studies; and (IV) the detection of intermediates and the proposition of degradation pathways. Although it is evident from most of the reviewed studies that several photo-combined AOP processes are efficient for the degradation of several classes of pharmaceutical compounds, the identification of intermediate products and toxicity levels are equally crucial, although they have been less explored in the literature, as these products can be more biologically active or toxic than their parent compounds, thus creating even greater hazards for the environment.

In addition, most of the literature discussed here is devoted to laboratory-scale or pilot-scale studies. The implementation of AOPs at a full scale is still quite limited. The major impediment to the application on an industrial scale is the elevated operational cost of combined AOP processes, mainly compared to conventional methods that are currently applied. Thus, if the overall cost per unit mass of pollutant removed from the unit volume of the treated wastewater is reduced, the industrial implementation of these technologies will become more appealing for companies and public administrations.

In summary, the literature of pharmaceutical compound degradation through advanced oxidation processes coupled with UV radiation has made some progress, and future research should focus on the following aspects to achieve these goals:

- More studies need to be carried out using real wastewater samples to evaluate the effectiveness of the combined advanced oxidative processes, since the matrix of real wastewater samples is complex due to the presence of organic and inorganic substances besides the variations of wastewater characteristics.
- Advanced oxidation processes need to be optimized to improve their adaptability and practicability, such as enhancing the efficiency and dosage of the photocatalysts and the utilization efficiency of O_3 or H_2O_2.
- Energy costs must also be reduced. In this context, the search for novel, affordable photocatalysts that can use a broader part of the light spectrum instead of only UV is a priority. Furthermore, the application of renewable energy sources in the treatment plants should also be investigated.
- The generation mechanism of free radicals and the degradation pathways of pollutants are not yet clear. More attention should be given to the study of mechanisms, combining experimental measurements with theoretical calculations.
- The generation of waste (e.g., sludge in the photo-Fenton process and/or exhausted or poisoned catalysts in photocatalyzed AOPs) should be minimized and possible alternatives for the valorization of such wastes should be explored.
- It is recommended that future studies should focus on the evaluation of treated water toxicity, employing ecotoxicity tests to monitor the toxicity of the by-products formed during the degradation.

Author Contributions: Conceptualization, I.M.D.G. and C.V.S.A.; methodology, I.M.D.G. and C.V.S.A.; formal analysis, I.M.D.G. and C.V.S.A.; resources, I.M.D.G., C.V.S.A. and L.H.M.; data curation, I.M.D.G., C.V.S.A. and L.H.M.; writing—original draft preparation, I.M.D.G. and C.V.S.A.; writing—review and editing, I.M.D.G., C.V.S.A. and L.H.M.; visualization, I.M.D.G., C.V.S.A. and L.H.M.; supervision, L.H.M.; project administration, L.H.M.; funding acquisition, L.H.M. All authors have read and agreed to the published version of the manuscript.

Funding: This research was funded by FAPESP (#2020/15211-0, #2021/14693-4), CEPID/FAPESP (#2013/07296-2), FAPESP/SHELL (#2017/11986-5).

Data Availability Statement: Not applicable.

Acknowledgments: The authors would like to thank FAPESP (#2020/15211-0, #2021/14693-4), CEPID/FAPESP (#2013/07296-2), FAPESP/SHELL (#2017/11986-5). The authors also thanks Shell and the strategic importance of the support given by ANP (Brazil's National Oil, Natural Gas and Biofuels Agency) through the R&D levy regulation, CNPq, CAPES finance code 001 and FINEP for the financial support.

Conflicts of Interest: The authors declare no conflict of interest.

References

1. Karimi-Maleh, H.; Karimi, F.; Fu, L.; Sanati, A.; Alizadeh, M.; Karaman, C.; Orooji, Y. Cyanazine herbicide monitoring as a hazardous substance by a DNA nanostructure biosensor. *J. Hazard. Mater.* **2022**, *423*, 127058. https://doi.org/10.1016/j.jhazmat.2021.127058.
2. Chandarana, H.; Kumar, P.S.; Seenuvasan, M.; Kumar, M.A. Kinetics, equilibrium and thermodynamic investigations of methylene blue dye removal using Casuarina equisetifolia pines. *Chemosphere* **2021**, *285*, 131480. https://doi.org/10.1016/j.chemosphere.2021.131480.

3. Talbot, J.; Nilsson, B. Pharmacovigilance in the pharmaceutical industry. *Br. J. Clin. Pharmacol.* **1998**, *45*, 427–431. https://doi.org/10.1046/j.1365-2125.1998.00713.x.
4. Mansouri, F.; Chouchene, K.; Roche, N.; Ksibi, M. Removal of pharmaceuticals from water by adsorption and advanced oxidation processes: State of the art and trends. *Appl. Sci.* **2021**, *11*, 6659. https://doi.org/10.3390/app11146659.
5. Szabó, R.; Megyeri, C.; Illés, E.; Gajda-Schrantz, K.; Mazellier, P.; Dombi, A. Phototransformation of ibuprofen and ketoprofen in aqueous solutions. *Chemosphere* **2011**, *84*, 1658–1663. https://doi.org/10.1016/j.chemosphere.2011.05.012.
6. Majumder, A.; Gupta, B.; Gupta, A. Pharmaceutically active compounds in aqueous environment: A status, toxicity and insights of remediation. *Environ. Res.* **2019**, *176*, 108542. https://doi.org/10.1016/j.envres.2019.108542.
7. Velempini, T.; Prabakaran, E.; Pillay, K. Recent developments in the use of metal oxides for photocatalytic degradation of pharmaceutical pollutants in water—A review. *Mater. Today Chem.* **2021**, *19*, 100380. https://doi.org/10.1016/j.mtchem.2020.100380.
8. Brillas, E. A review on the degradation of organic pollutants in waters by UV photoelectro-fenton and solar photoelectro-fenton. *J. Braz. Chem. Soc.* **2014**, *25*, 393–417. https://doi.org/10.5935/0103-5053.20130257.
9. Martínez-Huitle, C.; Rodrigo, M.; Sirés, I.; Scialdone, O. Single and Coupled Electrochemical Processes and Reactors for the Abatement of Organic Water Pollutants: A Critical Review. *Chem. Rev.* **2015**, *115*, 13362–13407. https://doi.org/10.1021/acs.chemrev.5b00361.
10. de O.S. Santos, G.; Gonzaga, I.; Dória, A.; Moratalla, A.; da Silva, R.; Eguiluz, K.; Salazar-Banda, G.; Saez, C.; Rodrigo, M. Testing and scaling-up of a novel Ti/$Ru_{0.7}Ti_{0.3}O_2$ mesh anode in a microfluidic flow-through reactor. *Chem. Eng. J.* **2020**, *398*, 125568. https://doi.org/10.1016/j.cej.2020.125568.
11. Karimi-Maleh, H.; Ranjbari, S.; Tanhaei, B.; Ayati, A.; Orooji, Y.; Alizadeh, M.; Karimi, F.; Salmanpour, S.; Rouhi, J.; Sillanpää, M.; et al. Novel 1-butyl-3-methylimidazolium bromide impregnated chitosan hydrogel beads nanostructure as an efficient nanobio-adsorbent for cationic dye removal: Kinetic study. *Environ. Res.* **2021**, *195*, 110809. https://doi.org/10.1016/j.envres.2021.110809.
12. Saravanan, A.; Kumar, P.; Jeevanantham, S.; Anubha, M.; Jayashree, S. Degradation of toxic agrochemicals and pharmaceutical pollutants: Effective and alternative approaches toward photocatalysis. *Environ. Pollut.* **2022**, *298*, 118844. https://doi.org/10.1016/j.envpol.2022.118844.
13. Moratalla, Á.; Cotillas, S.; Lacasa, E.; Fernández-Marchante, C.; Ruiz, S.; Valladolid, A.; Cañizares, P.; Rodrigo, M.; Sáez, C. Occurrence and toxicity impact of pharmaceuticals in hospital effluents: Simulation based on a case of study. *Process Saf. Environ. Prot.* **2022**, *168*, 10–21. https://doi.org/10.1016/j.psep.2022.09.066.
14. Jelic, A.; Cruz-Morató, C.; Marco-Urrea, E.; Sarrà, M.; Perez, S.; Vicent, T.; Petrović, M.; Barcelo, D. Degradation of carbamazepine by Trametes versicolor in an air pulsed fluidized bed bioreactor and identification of intermediates. *Water Res.* **2012**, *46*, 955–964. https://doi.org/10.1016/j.watres.2011.11.063.
15. Ahuja, S. Current status of pharmaceutical contamination in water, in: Handb. *Water Purity Qual.* **2021**, 255–270. https://doi.org/10.1016/b978-0-12-821057-4.00008-2.
16. Li, M.; An, Z.; Huo, Y.; Jiang, J.; Zhou, Y.; Cao, H.; Jin, Z.; Xie, J.; Zhan, J.; He, M. Individual and combined degradation of N-heterocyclic compounds under sulfate radical-based advanced oxidation processes. *Chem. Eng. J.* **2022**, *442*, 136316. https://doi.org/10.1016/j.cej.2022.136316.
17. Yao, J.; Tang, Y.; Zhang, Y.; Ruan, M.; Wu, W.; Sun, J. New theoretical investigation of mechanism, kinetics, and toxicity in the degradation of dimetridazole and ornidazole by hydroxyl radicals in aqueous phase. *J. Hazard. Mater.* **2022**, *422*, 126930. https://doi.org/10.1016/j.jhazmat.2021.126930.
18. Li, B.; Ma, X.; Deng, J.; Li, Q.; Chen, W.; Li, G.; Chen, G.; Wang, J. Comparison of acetaminophen degradation in UV-LED-based advance oxidation processes: Reaction kinetics, radicals contribution, degradation pathways and acute toxicity assessment. *Sci. Total Environ.* **2020**, *723*, 137993. https://doi.org/10.1016/j.scitotenv.2020.137993.
19. Cai, H.; Zou, J.; Lin, J.; Li, J.; Huang, Y.; Zhang, S.; Ma, J. Sodium hydroxide-enhanced acetaminophen elimination in heat/peroxymonosulfate system: Production of singlet oxygen and hydroxyl radical. *Chem. Eng. J.* **2022**, *429*, 132438. https://doi.org/10.1016/j.cej.2021.132438.
20. Cai, H.; Zou, J.; Lin, J.; Li, Q.; Li, J.; Huang, Y.; Ma, J. Elimination of acetaminophen in sodium carbonate-enhanced thermal/peroxymonosulfate process: Performances, influencing factors and mechanism. *Chem. Eng. J.* **2022**, *449*, 137765. https://doi.org/10.1016/j.cej.2022.137765.
21. Li, J.; Zou, J.; Zhang, S.; Cai, H.; Huang, Y.; Lin, J.; Ma, J. Sodium tetraborate simultaneously enhances the degradation of acetaminophen and reduces the formation potential of chlorinated by-products with heat-activated peroxymonosulfate oxidation. *Water Res.* **2022**, *224*, 119095.
22. Li, Q.; Zhang, M.; Xu, Y.; Quan, X.; Xu, Y.; Liu, W.; Wang, L. Constructing heterojunction interface of Co_3O_4/TiO_2 for efficiently accelerating acetaminophen degradation via photocatalytic activation of sulfite. *Chin. Chem. Lett.* **2022**, *34*, 107530. https://doi.org/10.1016/j.cclet.2022.05.044.
23. Sayadi, M.; Sobhani, S.; Shekari, H. Photocatalytic degradation of azithromycin using GO@Fe_3O_4/ ZnO/ SnO_2 nanocomposites. *J. Clean. Prod.* **2019**, *232*, 127–136. https://doi.org/10.1016/j.jclepro.2019.05.338.
24. Tenzin, T.; Yashas, S.; Anilkumar, K.; Shivaraju, H. UV–LED driven photodegradation of organic dye and antibiotic using strontium titanate nanostructures. *J. Mater. Sci. Mater. Electron.* **2021**, *32*, 21093–21105. https://doi.org/10.1007/s10854-021-06609-8.

25. Martins, P.; Salazar, H.; Aoudjit, L.; Gonçalves, R.; Zioui, D.; Fidalgo-Marijuan, A.; Costa, C.; Ferdov, S.; Lanceros-Mendez, S. Crystal morphology control of synthetic giniite for enhanced photo-Fenton activity against the emerging pollutant metronidazole. *Chemosphere* **2021**, *262*, 128300. https://doi.org/10.1016/j.chemosphere.2020.128300.
26. Neghi, N.; Krishnan, N.; Kumar, M. Analysis of metronidazole removal and micro-toxicity in photolytic systems: Effects of persulfate dosage, anions and reactor operation-mode. *J. Environ. Chem. Eng.* **2018**, *6*, 754–761. https://doi.org/10.1016/j.jece.2017.12.072.
27. Leeladevi, K.; Kumar, J.V.; Arunpandian, M.; Thiruppathi, M.; Nagarajan, E. Investigation on photocatalytic degradation of hazardous chloramphenicol drug and amaranth dye by $SmVO_4$ decorated g-C_3N_4 nanocomposites. *Mater. Sci. Semicond. Process.* **2021**, *123*, 105563. https://doi.org/10.1016/j.mssp.2020.105563.
28. Hu, X.; Qin, J.; Wang, Y.; Wang, J.; Yang, A.; Tsang, Y.; Liu, B. Synergic degradation Chloramphenicol in photo-electrocatalytic microbial fuel cell over Ni/MXene photocathode. *J. Colloid Interface Sci.* **2022**, *628*, 327–337. https://doi.org/10.1016/j.jcis.2022.08.040.
29. Kumar, A.; Sharma, S.; Kumar, A.; Sharma, G.; AlMasoud, N.; Alomar, T.; Naushad, M.; ALOthman, Z.; Stadler, F. High interfacial charge carrier separation in Fe_3O_4 modified $SrTiO_3$/$Bi_4O_5I_2$ robust magnetic nano-heterojunction for rapid photodegradation of diclofenac under simulated solar-light. *J. Clean. Prod.* **2021**, *315*, 128137. https://doi.org/10.1016/j.jclepro.2021.128137.
30. Li, S.; Cui, J.; Wu, X.; Zhang, X.; Hu, Q.; Hou, X. Rapid in situ microwave synthesis of Fe3O4@MIL-100(Fe) for aqueous diclofenac sodium removal through integrated adsorption and photodegradation. *J. Hazard. Mater.* **2019**, *373*, 408–416. https://doi.org/10.1016/j.jhazmat.2019.03.102.
31. Gonzaga, I.; Dória, A.; Moratalla, A.; Eguiluz, K.; Salazar-Banda, G.; Cañizares, P.; Rodrigo, M.; Saez, C. Electrochemical systems equipped with 2D and 3D microwave-made anodes for the highly efficient degradation of antibiotics in urine. *Electrochim. Acta.* **2021**, *392*, 139012. https://doi.org/10.1016/j.electacta.2021.139012.
32. Kumari, A.; Kumar, A.; Sharma, G.; Iqbal, J.; Naushad, M.; Stadler, F. Constructing Z-scheme $LaTiO_2N$/g-C_3N_4@Fe_3O_4 magnetic nano heterojunctions with promoted charge separation for visible and solar removal of indomethacin. *J. Water Process Eng.* **2020**, *36*, 101391. https://doi.org/10.1016/j.jwpe.2020.101391.
33. Li, R.; Kong, J.; Liu, H.; Chen, P.; Su, Y.; Liu, G.; Lv, W. Removal of indomethacin using UV–vis/peroxydisulfate: Kinetics, toxicity, and transformation pathways. *Chem. Eng. J.* **2018**, *331*, 809–817. https://doi.org/10.1016/j.cej.2017.09.025.
34. Cao, J.; Li, J.; Chu, W.; Cen, W. Facile synthesis of Mn-doped BiOCl for metronidazole photodegradation: Optimization, degradation pathway, and mechanism. *Chem. Eng. J.* **2020**, *400*, 125813. https://doi.org/10.1016/j.cej.2020.125813.
35. Parra-Enciso, C.; Avila, B.; Rubio-Clemente, A.; Peñuela, G. Degradation of diclofenac through ultrasonic-based advanced oxidation processes at low frequency. *J. Environ. Chem. Eng.* **2022**, *10*, 108296. https://doi.org/10.1016/j.jece.2022.108296.
36. Naraginti, S.; Yu, Y.; Fang, Z.; Yong, Y. Visible light degradation of macrolide antibiotic azithromycin by novel ZrO_2/Ag@TiO_2 nanorod composite: Transformation pathways and toxicity evaluation. *Process Saf. Environ. Prot.* **2019**, *125*, 39–49. https://doi.org/10.1016/j.psep.2019.02.031.
37. Cano, P.; Jaramillo-Baquero, M.; Zúñiga-Benítez, H.; Londoño, Y.; Peñuela, G. Use of simulated sunlight radiation and hydrogen peroxide in azithromycin removal from aqueous solutions: Optimization & mineralization analysis. *Emerg. Contam.* **2020**, *6*, 53–61. https://doi.org/10.1016/j.emcon.2019.12.004.
38. de Almeida, L.; Josué, T.; Fidelis, M.; Abreu, E.; Bechlin, M.; Santos, O.; Lenzi, G. Process Comparison for Caffeine Degradation: Fenton, Photo-Fenton, UV/H_2O_2 and UV/Fe^{3+}. *Water. Air. Soil Pollut.* **2021**, *232*, 147. https://doi.org/10.1007/s11270-021-05115-1.
39. Goulart, L.; Moratalla, A.; Cañizares, P.; Lanza, M.; Sáez, C.; Rodrigo, M. High levofloxacin removal in the treatment of synthetic human urine using Ti/MMO/ZnO photo-electrocatalyst. *J. Environ. Chem. Eng.* **2022**, *10*, 107317. https://doi.org/10.1016/j.jece.2022.107317.
40. Geng, C.; Liang, Z.; Cui, F.; Zhao, Z.; Yuan, C.; Du, J.; Wang, C. Energy-saving photo-degradation of three fluoroquinolone antibiotics under VUV/UV irradiation: Kinetics, mechanism, and antibacterial activity reduction. *Chem. Eng. J.* **2020**, *383*, 123145. https://doi.org/10.1016/j.cej.2019.123145.
41. Jia, J.; Guan, Y.; Cheng, M.; Chen, H.; He, J.; Wang, S.; Wang, Z. Occurrence and distribution of antibiotics and antibiotic resistance genes in Ba River. *China Sci. Total Environ.* **2018**, *642*, 1136–1144. https://doi.org/10.1016/j.scitotenv.2018.06.149.
42. Wormser, G.; Tang, Y.-W. Antibiotics in Laboratory Medicine, 5th Edition Edited by Victor Lorain Philadelphia: Lippincott Williams & Wilkins, 2005 832 pp. illustrated. $199.00 (cloth). *Clin. Infect. Dis.* **2005**, *41*, 577–577. https://doi.org/10.1086/432067.
43. Liu, X.; Lu, S.; Guo, W.; Xi, B.; Wang, W. Antibiotics in the aquatic environments: A review of lakes. *China Sci. Total Environ.* **2018**, *627*, 1195–1208. https://doi.org/10.1016/j.scitotenv.2018.01.271.
44. He, K.; Hain, E.; Timm, A.; Tarnowski, M.; Blaney, L. Occurrence of antibiotics, estrogenic hormones, and UV-filters in water, sediment, and oyster tissue from the Chesapeake Bay. *Sci. Total Environ.* **2019**, *650*, 3101–3109. https://doi.org/10.1016/j.scitotenv.2018.10.021.
45. Boy-Roura, M.; Mas-Pla, J.; Petrovic, M.; Gros, M.; Soler, D.; Brusi, D.; Menció, A. Towards the understanding of antibiotic occurrence and transport in groundwater: Findings from the Baix Fluvià alluvial aquifer (NE Catalonia, Spain). *Sci. Total Environ.* **2018**, *612*, 1387–1406. https://doi.org/10.1016/j.scitotenv.2017.09.012.
46. Wu, M.; Que, C.; Xu, G.; Sun, Y.; Ma, J.; Xu, H.; Sun, R.; Tang, L. Occurrence, fate and interrelation of selected antibiotics in sewage treatment plants and their receiving surface water. *Ecotoxicol. Environ. Saf.* **2016**, *132*, 132–139. https://doi.org/10.1016/j.ecoenv.2016.06.006.

47. Mondal, S.; Saha, A.; Sinha, A. Removal of ciprofloxacin using modified advanced oxidation processes: Kinetics, pathways and process optimization. *J. Clean. Prod.* **2018**, *171*, 1203–1214. https://doi.org/10.1016/j.jclepro.2017.10.091.
48. Liu, X.; Liu, Y.; Lu, S.; Wang, Z.; Wang, Y.; Zhang, G.; Guo, X.; Guo, W.; Zhang, T.; Xi, B. Degradation difference of ofloxacin and levofloxacin by UV/H_2O_2 and UV/PS (persulfate): Efficiency, factors and mechanism. *Chem. Eng. J.* **2019**, *385*, 123987. https://doi.org/10.1016/j.cej.2019.123987.
49. Wang, C.; Zhang, J.; Du, J.; Zhang, P.; Zhao, Z.; Shi, W.; Cui, F. Rapid degradation of norfloxacin by VUV/Fe^{2+}/H_2O_2 over a wide initial pH: Process parameters, synergistic mechanism, and influencing factors. *J. Hazard. Mater.* **2021**, *416*, 125893. https://doi.org/10.1016/j.jhazmat.2021.125893.
50. Yao, W.; Rehman, S.U.; Wang, H.; Yang, H.; Yu, G.; Wang, Y. Pilot-scale evaluation of micropollutant abatements by conventional ozonation, UV/O_3, and an electro-peroxone process. *Water Res.* **2018**, *138*, 106–117. https://doi.org/10.1016/j.watres.2018.03.044.
51. Liu, H.; Gao, Y.; Wang, J.; Ma, D.; Wang, Y.; Gao, B.; Yue, Q.; Xu, X. The application of UV/O_3 process on ciprofloxacin wastewater containing high salinity: Performance and its degradation mechanism. *Chemosphere* **2021**, *276*, 130220. https://doi.org/10.1016/j.chemosphere.2021.130220.
52. Paucar, N.E.; Kim, I.; Tanaka, H.; Sato, C. Effect of O_3 dose on the O_3/UV treatment process for the removal of pharmaceuticals and personal care products in secondary effluent. *Chem. Eng.* **2019**, *3*, 53. https://doi.org/10.3390/chemengineering3020053.
53. Asgari, E.; Sheikhmohammadi, A.; Nourmoradi, H.; Nazari, S.; Aghanaghad, M. Degradation of ciprofloxacin by photocatalytic ozonation process under irradiation with UVA: Comparative study, performance and mechanism. *Process Saf. Environ. Prot.* **2021**, *147*, 356–366. https://doi.org/10.1016/j.psep.2020.09.041.
54. Ghattavi, S.; Nezamzadeh-Ejhieh, A. A double-Z-scheme ZnO/AgI/WO_3 photocatalyst with high visible light activity: Experimental design and mechanism pathway in the degradation of methylene blue. *J. Mol. Liq.* **2021**, *322*, 114563. https://doi.org/10.1016/j.molliq.2020.114563.
55. Costa, L.; Nobre, F.; Lobo, A.; de Matos, J. Photodegradation of ciprofloxacin using Z-scheme TiO_2/SnO_2 nanostructures as photocatalyst. *Environ. Nanotechnol. Monit. Manag.* **2021**, *16*, 100466. https://doi.org/10.1016/j.enmm.2021.100466.
56. Nguyen, L.; Nguyen, H.; Pham, T.; Tran, T.; Chu, H.; Dang, H.; Nguyen, V.; Nguyen, K.; Pham, T.; Van der Bruggen, B. UV–Visible Light Driven Photocatalytic Degradation of Ciprofloxacin by N,S Co-doped TiO_2: The Effect of Operational Parameters. *Top. Catal.* **2020**, *63*, 985–995. https://doi.org/10.1007/s11244-020-01319-7.
57. Zhang, M.; Lai, C.; Li, B.; Huang, D.; Liu, S.; Qin, L.; Yi, H.; Fu, Y.; Xu, F.; Li, M.; et al. Ultrathin oxygen-vacancy abundant WO_3 decorated monolayer Bi_2WO_6 nanosheet: A 2D/2D heterojunction for the degradation of Ciprofloxacin under visible and NIR light irradiation. *J. Colloid Interface Sci.* **2019**, *556*, 557–567. https://doi.org/10.1016/j.jcis.2019.08.101.
58. Wu, D.; Li, J.; Guan, J.; Liu, C.; Zhao, X.; Zhu, Z.; Ma, C.; Huo, P.; Li, C.; Yan, Y. Improved photoelectric performance via fabricated heterojunction g-C_3N_4/TiO_2/HNTs loaded photocatalysts for photodegradation of ciprofloxacin. *J. Ind. Eng. Chem.* **2018**, *64*, 206–218. https://doi.org/10.1016/j.jiec.2018.03.017.
59. Prabavathi, S.; Saravanakumar, K.; Park, C.; Muthuraj, V. Photocatalytic degradation of levofloxacin by a novel Sm_6WO_{12}/g-C_3N_4 heterojunction: Performance, mechanism and degradation pathways. *Sep. Purif. Technol.* **2021**, *257*, 117985. https://doi.org/10.1016/j.seppur.2020.117985.
60. Al Balushi, B.; Al Marzouqi, F.; Al Wahaibi, B.; Kuvarega, A.; Al Kindy, S.; Kim, Y.; Selvaraj, R. Hydrothermal synthesis of CdS sub-microspheres for photocatalytic degradation of pharmaceuticals. *Appl. Surf. Sci.* **2018**, *457*, 559–565. https://doi.org/10.1016/j.apsusc.2018.06.286.
61. Lu, G.; Lun, Z.; Liang, H.; Wang, H.; Li, Z.; Ma, W. In situ fabrication of $BiVO_4$-$CeVO_4$ heterojunction for excellent visible light photocatalytic degradation of levofloxacin. *J. Alloys Compd.* **2019**, *772*, 122–131. https://doi.org/10.1016/j.jallcom.2018.09.064.
62. Zhang, X.; Zhang, Y.; Jia, X.; Zhang, N.; Xia, R.; Zhang, X.; Wang, Z.; Yu, M. In situ fabrication of a novel S-scheme heterojunction photocatalyts Bi_2O_3/P-C_3N_4 to enhance levofloxacin removal from water. *Sep. Purif. Technol.* **2021**, *268*, 118691. https://doi.org/10.1016/j.seppur.2021.118691.
63. Aghaeinejad-Meybodi, A.; Ebadi, A.; Shafiei, S.; Khataee, A.; Kiadehi, A. Degradation of Fluoxetine using catalytic ozonation in aqueous media in the presence of nano-Γ-alumina catalyst: Experimental, modeling and optimization study. *Sep. Purif. Technol.* **2019**, *211*, 551–563. https://doi.org/10.1016/j.seppur.2018.10.020.
64. Pan, C.; Zhu, F.; Wu, M.; Jiang, L.; Zhao, X.; Yang, M. Degradation and toxicity of the antidepressant fluoxetine in an aqueous system by UV irradiation. *Chemosphere* **2022**, *287*, 132434. https://doi.org/10.1016/j.chemosphere.2021.132434.
65. Hollman, J.; Dominic, J.; Achari, G. Degradation of pharmaceutical mixtures in aqueous solutions using UV/peracetic acid process: Kinetics, degradation pathways and comparison with UV/H_2O_2. *Chemosphere* **2020**, *248*, 125911. https://doi.org/10.1016/j.chemosphere.2020.125911.
66. Szabó, L.; Mile, V.; Kiss, D.; Kovács, K.; Földes, T.; Németh, T.; Tóth, T.; Homlok, R.; Balogh, G.; Takács, E.; et al. Applicability evaluation of advanced processes for elimination of neurophysiological activity of antidepressant fluoxetine. *Chemosphere* **2018**, *193*, 489–497. https://doi.org/10.1016/j.chemosphere.2017.11.047.
67. Sharma, S.; Kumar, A.; Sharma, G.; Naushad, M.; Vo, D.; Alam, M.; Stadler, F. Fe_3O_4 mediated Z-scheme $BiVO_4$/$Cr_2V_4O_{13}$ strongly coupled nano-heterojunction for rapid degradation of fluoxetine under visible light. *Mater. Lett.* **2020**, *281*, 128650. https://doi.org/10.1016/j.matlet.2020.128650.

68. Norouzi, R.; Zarei, M.; Khataee, A.; Ebratkhahan, M.; Rostamzadeh, P. Electrochemical removal of fluoxetine via three mixed metal oxide anodes and carbonaceous cathodes from contaminated water. *Environ. Res.* **2022**, *207*, 112641. https://doi.org/10.1016/j.envres.2021.112641.
69. Acosta-Rangel, A.; Sánchez-Polo, M.; Polo, A.; Rivera-Utrilla, J.; Berber-Mendoza, M. Sulfonamides degradation assisted by UV, UV/H_2O_2 and UV/$K_2S_2O_8$: Efficiency, mechanism and byproducts cytotoxicity. *J. Environ. Manag.* **2018**, *225*, 224–231. https://doi.org/10.1016/j.jenvman.2018.06.097.
70. Moradi, M.; Moussavi, G. Investigation of chemical-less UVC/VUV process for advanced oxidation of sulfamethoxazole in aqueous solutions: Evaluation of operational variables and degradation mechanism. *Sep. Purif. Technol.* **2018**, *190*, 90–99. https://doi.org/10.1016/j.seppur.2017.08.006.
71. Wen, D.; Wu, Z.; Tang, Y.; Li, M.; Qiang, Z. Accelerated degradation of sulfamethazine in water by VUV/UV photo-Fenton process: Impact of sulfamethazine concentration on reaction mechanism. *J. Hazard. Mater.* **2018**, *344*, 1181–1187. https://doi.org/10.1016/j.jhazmat.2017.10.032.
72. Hong, M.; Wang, Y.; Lu, G. UV-Fenton degradation of diclofenac, sulpiride, sulfamethoxazole and sulfisomidine: Degradation mechanisms, transformation products, toxicity evolution and effect of real water matrix. *Chemosphere* **2020**, *258*, 127351. https://doi.org/10.1016/j.chemosphere.2020.127351.
73. Jia, M.; Yang, Z.; Xu, H.; Song, P.; Xiong, W.; Cao, J.; Zhang, Y.; Xiang, Y.; Hu, J.; Zhou, C.; et al. Integrating N and F co-doped TiO_2 nanotubes with ZIF-8 as photoelectrode for enhanced photo-electrocatalytic degradation of sulfamethazine. *Chem. Eng. J.* **2020**, *388*, 124388. https://doi.org/10.1016/j.cej.2020.124388.
74. Teng, W.; Xu, J.; Cui, Y.; Yu, J. Photoelectrocatalytic degradation of sulfadiazine by Ag_3PO_4/MoS_2/TiO_2 nanotube array electrode under visible light irradiation. *J. Electroanal. Chem.* **2020**, *868*, 114178. https://doi.org/10.1016/j.jelechem.2020.114178.
75. She, S.; Wang, Y.; Chen, R.; Yi, F.; Sun, C.; Hu, J.; Li, Z.; Lu, G.; Zhu, M. Ultrathin S-doped graphitic carbon nitride nanosheets for enhanced sulpiride degradation via visible-light-assisted peroxydisulfate activation: Performance and mechanism. *Chemosphere* **2021**, *266*, 128929. https://doi.org/10.1016/j.chemosphere.2020.128929.
76. Zhang, Y.; Xiao, Y.; Zhong, Y.; Lim, T. Comparison of amoxicillin photodegradation in the UV/H_2O_2 and UV/persulfate systems: Reaction kinetics, degradation pathways, and antibacterial activity. *Chem. Eng. J.* **2019**, *372*, 420–428. https://doi.org/10.1016/j.cej.2019.04.160.
77. Lu, J.; Ji, Y.; Chovelon, J.; Lu, J. Fluoroquinolone antibiotics sensitized photodegradation of isoproturon. *Water Res.* **2021**, *198*, 117136. https://doi.org/10.1016/j.watres.2021.117136.
78. Wan, Z.; Wang, J. Removal of sulfonamide antibiotics from wastewater by gamma irradiation in presence of iron ions. *Nucl. Sci. Tech.* **2016**, *27*, 104. https://doi.org/10.1007/s41365-016-0109-3.
79. Lin, C.; Wu, M. Feasibility of using UV/H_2O_2 process to degrade sulfamethazine in aqueous solutions in a large photoreactor. *J. Photochem. Photobiol. A Chem.* **2018**, *367*, 446–451. https://doi.org/10.1016/j.jphotochem.2018.08.044.
80. Aryee, A.; Han, R.; Qu, L. Occurrence, detection and removal of amoxicillin in wastewater: A review. *J. Clean. Prod.* **2022**, *368*, 133140. https://doi.org/10.1016/j.jclepro.2022.133140.
81. Yazidi, A.; Atrous, M.; Soetaredjo, F.E.; Sellaoui, L.; Ismadji, S.; Erto, A.; Bonilla-Petriciolet, A.; Dotto, G.L.; Lamine, A.B. Adsorption of amoxicillin and tetracycline on activated carbon prepared from durian shell in single and binary systems: Experimental study and modeling analysis. *Chem. Eng. J.* **2020**, *379*, 122320. https://doi.org/10.1016/j.cej.2019.122320.
82. Ighalo, J.; Igwegbe, C.; Aniagor, C.; Oba, S. A review of methods for the removal of penicillins from water. *J. Water Process Eng.* **2021**, *39*, 101886. https://doi.org/10.1016/j.jwpe.2020.101886.
83. Verma, M.; Haritash, A. Degradation of amoxicillin by Fenton and Fenton-integrated hybrid oxidation processes. *J. Environ. Chem. Eng.* **2019**, *7*, 102886. https://doi.org/10.1016/j.jece.2019.102886.
84. Le, S.; Zhu, C.; Cao, Y.; Wang, P.; Liu, Q.; Zhou, H.; Chen, C.; Wang, S.; Duan, X. V_2O_5 nanodot-decorated laminar C_3N_4 for sustainable photodegradation of amoxicillin under solar light, Appl. *Catal. B Environ.* **2022**, *303*, 120903. https://doi.org/10.1016/j.apcatb.2021.120903.
85. Guerra, M.H.; Alberola, I.O.; Rodriguez, S.M.; López, A.A.; Merino, A.A.; Lopera, A.E.-C.; Alonso, J.Q. Oxidation mechanisms of amoxicillin and paracetamol in the photo-Fenton solar process. *Water Res.* **2019**, *156*, 232–240. https://doi.org/10.1016/j.watres.2019.02.055.
86. Mmelesi, O.; Patala, R.; Nkambule, T.; Mamba, B.; Kefeni, K.; Kuvarega, A. Effect of Zn doping on physico-chemical properties of cobalt ferrite for the photodegradation of amoxicillin and deactivation of *E. coli*. *Colloids Surf. A Physicochem. Eng. Asp.* **2022**, *649*, 129462. https://doi.org/10.1016/j.colsurfa.2022.129462.
87. Freitas, J.; Quintão, F.; da Silva, J.; de Queiroz, S.; Aquino, S.; de Cássia Franco, R.J. Characterisation of captopril photolysis and photocatalysis by-products in water by direct infusion, electrospray ionisation, high-resolution mass spectrometry and the assessment of their toxicities. *Int. J. Environ. Anal. Chem.* **2017**, *97*, 42–55. https://doi.org/10.1080/03067319.2016.1276578.
88. Santos, A.; Cabot, P.; Brillas, E.; Sirés, I. A comprehensive study on the electrochemical advanced oxidation of antihypertensive captopril in different cells and aqueous matrices. *Appl. Catal. B Environ.* **2020**, *277*, 119240. https://doi.org/10.1016/j.apcatb.2020.119240.
89. Osawa, R.A.; Barrocas, B.T.; Monteiro, O.C.; Oliveira, M.; Florêncio, M. Photocatalytic degradation of cyclophosphamide and ifosfamide: Effects of wastewater matrix, transformation products and in silico toxicity prediction. *Sci. Total Environ.* **2019**, *692*, 503–510. https://doi.org/10.1016/j.scitotenv.2019.07.247.

90. Russo, C.; Lavorgna, M.; Česen, M.; Kosjek, T.; Heath, E.; Isidori, M. Evaluation of acute and chronic ecotoxicity of cyclophosphamide, ifosfamide, their metabolites/transformation products and UV treated samples. *Environ. Pollut.* **2018**, *233*, 356–363. https://doi.org/10.1016/j.envpol.2017.10.066.
91. Janssens, R.; Cristovao, M.; Bronze, M.; Crespo, J.; Pereira, V.; Luis, P. Coupling of nanofiltration and UV, UV/TiO_2 and UV/H_2O_2 processes for the removal of anti-cancer drugs from real secondary wastewater effluent. *J. Environ. Chem. Eng.* **2019**, *7*, 103351, https://doi.org/10.1016/j.jece.2019.103351.
92. Graumans, M.; Hoeben, W.; Russel, F.; Scheepers, P. Oxidative degradation of cyclophosphamide using thermal plasma activation and UV/H_2O_2 treatment in tap water. *Environ. Res.* **2020**, *182*, 109046. https://doi.org/10.1016/j.envres.2019.109046.
93. Sabouni, R.; Murtaza, S.; Ghommem, M. Facile Metal Organic Framework Composites as Photocatalysts for Lone/Simultaneous Photodegradation of Naproxen, Ibuprofen and Methyl Orange. *SSRN Electron. J.* **2022**, *27*, 102751. https://doi.org/10.2139/ssrn.4015288.
94. Wu, T.; Pi, M.; Zhang, D.; Chen, S. Three-dimensional porous structural MoP_2 nanoparticles as a novel and superior catalyst for electrochemical hydrogen evolution. *J. Power Source* **2016**, *328*, 551–557. https://doi.org/10.1016/j.jpowsour.2016.08.050.
95. Mohamed, A.; Salama, A.; Nasser, W.; Uheida, A. Photodegradation of Ibuprofen, Cetirizine, and Naproxen by PAN-MWCNT/TiO_2–NH_2 nanofiber membrane under UV light irradiation. *Environ. Sci. Eur.* **2018**, *30*, 47. https://doi.org/10.1186/s12302-018-0177-6.
96. Zhen, H.; Liu, J.; Zhang, T. The Effect of UV Degradation of Ketoprofen and Its Influencing Factors. *J. Phys. Conf. Ser.* **2022**, *2194*, 012049. https://doi.org/10.1088/1742-6596/2194/1/012049.
97. Mofokeng, L.; Hlekelele, L.; Tetana, Z.; Moma, J.; Chauke, V. CuO-doped TiO_2 Supported on Graphitic Carbon Nitride for the Photodegradation of Ketoprofen in Drinking and Groundwater: Process Optimization and Energy Consumption evaluation. *Chem. Select.* **2022**, *7*, e202101847. https://doi.org/10.1002/slct.202101847.
98. Chaker, H.; Fourmentin, S.; Chérif-Aouali, L. Efficient Photocatalytic Degradation of Ibuprofen under Visible Light Irradiation Using Silver and Cerium Co-Doped Mesoporous TiO_2. *Chem. Select.* **2020**, *5*, 11787–11796. https://doi.org/10.1002/slct.202002730.
99. Wang, P.; Bu, L.; Wu, Y.; Ma, W.; Zhu, S.; Zhou, S. Mechanistic insight into the degradation of ibuprofen in UV/H_2O_2 process via a combined experimental and DFT study. *Chemosphere* **2021**, *267*, 128883. https://doi.org/10.1016/j.chemosphere.2020.128883.
100. Cunha-Filho, F.; Mota-Lima, A.; Ratkievicius, L.; Silva, D.; Silva, D.; Chiavone-Filho, O.; Nascimento, C.O. Rapid mineralization rate of acetylsalicylic acid in a tubular photochemical reactor: The role of the optimized excess of H_2O_2. *J. Water Process Eng.* **2019**, *31*, 100856. https://doi.org/10.1016/j.jwpe.2019.100856.
101. Zhe, W.; Wenjuan, Z.; Haihan, W.; Zhiwei, W.; Jing, C. Oxidation of acetylsalicylic acid in water by UV/O_3 process: Removal, byproduct analysis, and investigation of degradation mechanism and pathway. *J. Environ. Chem. Eng.* **2021**, *9*, 106259. https://doi.org/10.1016/j.jece.2021.106259.
102. Karimi, P.; Baneshi, M.; Malakootian, M. Photocatalytic degradation of aspirin from aqueous solutions using the UV/ZnO process: Modelling, analysis and optimization by response surface methodology (RSM), Desalin. *Water Treat.* **2019**, *161*, 354–364. https://doi.org/10.5004/dwt.2019.24317.
103. Mohan, H.; Yoo, S.; Thimmarayan, S.; Oh, H.; Kim, G.; Seralathan, K.; Shin, T. Nickel decorated manganese oxynitride over graphene nanosheets as highly efficient visible light driven photocatalysts for acetylsalicylic acid degradation. *Environ. Pollut.* **2021**, *289*, 117864. https://doi.org/10.1016/j.envpol.2021.117864.
104. Pan, M.; Wu, Z.; Tang, C.; Guo, K.; Cao, Y.; Fang, J. Emerging investigators series: Comparative study of naproxen degradation by the UV/chlorine and the UV/H_2O_2 advanced oxidation processes. *Environ. Sci. Water Res. Technol.* **2018**, *4*, 1219–1230. https://doi.org/10.1039/c8ew00105g.
105. Zhou, S.; Li, L.; Wu, Y.; Zhu, S.; Zhu, N.; Bu, L.; Dionysiou, D. UV365 induced elimination of contaminants of emerging concern in the presence of residual nitrite: Roles of reactive nitrogen species. *Water Res.* **2020**, *178*, 115829. https://doi.org/10.1016/j.watres.2020.115829.
106. Tahir, M.; Sagir, M.; Shahzad, K. Removal of acetylsalicylate and methyl-theobromine from aqueous environment using nano-photocatalyst WO_3-TiO_2 @g-C_3N_4 composite. *J. Hazard. Mater.* **2018**, *363*, 205–213. https://doi.org/10.1016/j.jhazmat.2018.09.055.